Study of the Structure and the Dynamics of Ge-Sb-Te Liquids

Study of the local order of Ge-Sb-Te liquids by neutron scattering and inelastic X-Ray scattering compared with ab initio simulations (in relation with the University of Liège, Belgium)

by

Thomas Dorin

Diploma work No. 36/2010
at Department of Materials and Manufacturing Technology
CHALMERS UNIVERSITY OF TECHNOLOGY
Göteborg, Sweden

Diploma work in the Master programme Advanced Engineering Materials

Performed at: Laboratoire des Matériaux et du Génie Physique (LMGP)
BP 257 – Grenoble INP Minatec - 3 parvis Louis Néel
38016 Grenoble

Supervisor(s):   Professor Françoise Hippert
Laboratoire des Matériaux et du Génie Physique (LMGP)
BP 257 – Grenoble INP Minatec - 3 parvis Louis Néel
38016 Grenoble

Examiner: Professor Maria Knutson Wedel
Department of Materials and Manufacturing Technology
Chalmers University of Technology, SE-412 96 Göteborg

Study of the structure and the Dynamics of Ge-Sb-Te Liquids

Study of the local order of Ge-Sb-Te liquids by neutron scattering and inelastic X-Ray scattering compared with ab initio simulations (in relation with the University of Liège, Belgium)

THOMAS DORIN

Study of the Structure and the Dynamics of Ge-Sb-Te Liquids

Study of the local order of Ge-Sb-Te liquids by neutron scattering and Inelastic X-Ray scattering compared with ab initio simulations (in relation with the University of Liège, Belgium)

THOMAS DORIN

Department of Materials and Manufacturing Technology
Chalmers University of Technology

SUMMARY

Some liquids Ge-Te, such as the eutectic alloy $Ge_{15}Te_{85}$, exhibit a decrease of their volume when the temperature increases just above their melting point. This negative thermal expansion (NTE) is accompanied with thermodynamic anomalies and important changes in the electrical conductivity. Simulations have shown that this NTE is associated with a distortion of the octahedral structure around Ge atoms. Conversely, it was shown that liquid $Ge_{15}Sb_{85}$ does not exhibit any anomaly. This thesis focused on the effect of substituting Sb to Te in $Ge_{15}Te_{85}$. The total structure factors were measured by neutron scattering on the 7C2 spectrometer at the LLB (Laboratory Léon Brillouin, Saclay). The analysis of the results from this experiment suggested that Sb does not kill off the anomaly. Indeed, when Sb is added to $Ge_{15}Te_{85}$, the melting temperature of the alloy is increased. As a result, the anomaly that could be seen in the liquid for $Ge_{15}Te_{85}$, is moved into the overcooled area for $Ge_{15}(Sb_xTe_{1-x})_{85}$ alloys with $0<x<0.5$ but what happens for alloys with $x>0.5$ remains uncertain.
The dynamics of liquid $Ge_{15}Te_{85}$ were measured by Inelastic X-Ray scattering on the ID28 beamline at the ESRF (Grenoble). The containment for the sample had to be invented for this experiment.
In the ternary Ge-Te-Sb phase diagram, some alloys are the subject of numerous studies, they are known as phase change materials. Those materials exhibit a rapid and reversible phase transition between an amorphous and a crystalline phase with different electronic properties. The anomaly in the liquid state and the transition in the PCM are both associated with important changes in the electronic properties. The relation between those transitions is discussed.

Keywords: Ge-Sb-Te, negative thermal expansion, neutron scattering, inelastic X-Ray scattering, thermodynamic anomaly, structure factor, pair distribution function.

Table of Contents

1   Introduction

1.1   Phase Change Materials (PCM)

A PCM is a material that has two phases, an amorphous one and a crystalline one. To be classified as a PCM, a material must meet several criteria such as a high-speed phase transition, a long thermal stability of the amorphous state, a large optical reflectivity change between the two states (for optical storage) or a large resistance change between the states (for resistive storage), a large cyclability of reversible transitions and a high chemical stability (ref. 1).

Knowledge of materials that exhibit a structural transformation between the amorphous and the crystalline phases under an electrical current or a laser beam is well established. However, a new interest arose recently for those materials, with the possibility to use PCM in non-volatile resistive memories such as phase change random access memory (PCRAM). An extended use of PCM for PCRAMs for computers would be revolutionary. For example, it could allow a computer to be switched on and be ready for use within seconds without having to take time to load. The first prototypes of this type of memory have already been made and the first products using PCM memories will be commercialised by the end of the year.

These materials are Ge-Sb-Te alloys. In figure 1, the ternary diagram of Ge-Sb-Te is depicted. An important group of PC alloys is located on the line going from GeTe to Sb_2Te_3. For instance, $GeSb_2Te_5$ has been used for Rewritable DVD's for more than 10 years.
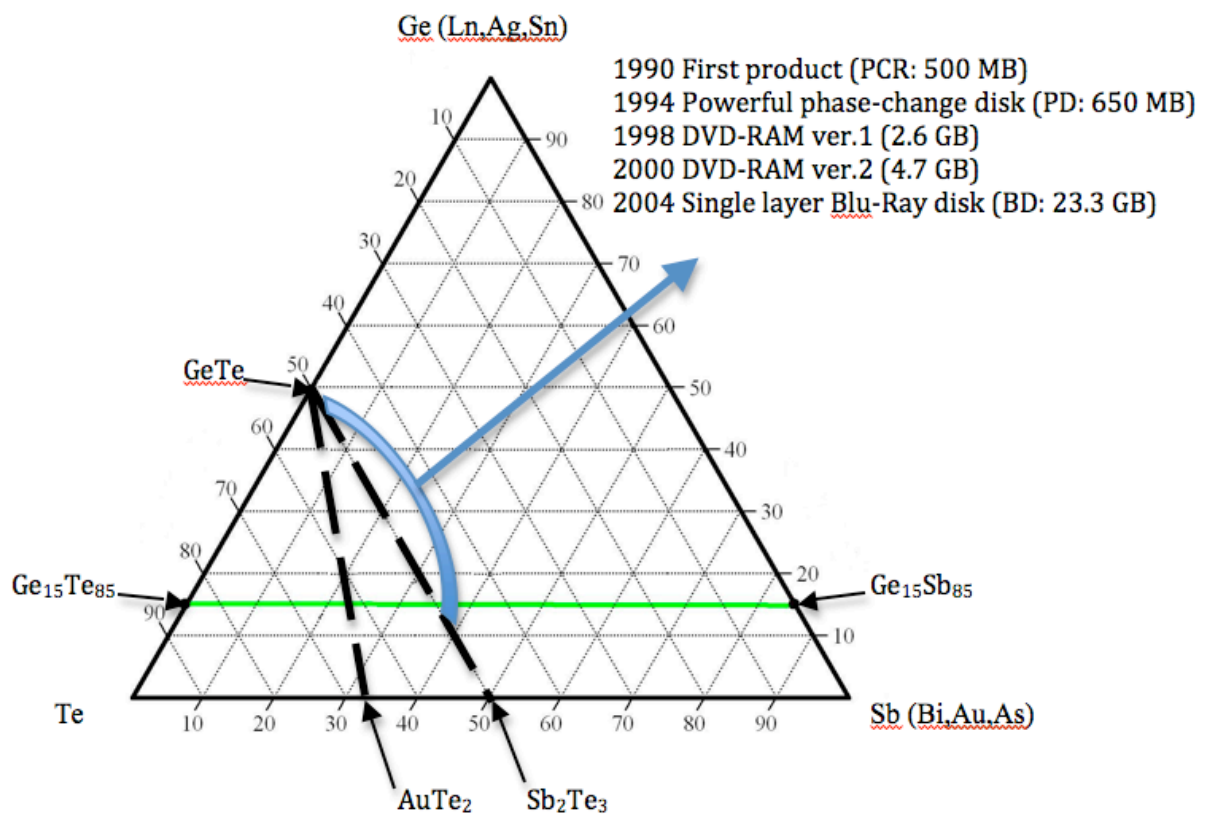

Figure 1: Ternary phase diagram depicting different phase-change alloys and their use in different optical storage products

The electrical data storage principle of PCRAMs is represented on Figure 2. With the help of an electrical pulse, the amorphous material is heated above the glass transition temperature (T_g) and then it rearranges into the crystalline state. To return to the amorphous state, a higher pulse is needed in order to heat the material above its melting temperature (T_m); it is then quenched in order to retain the amorphous state. The ratio $T_{rg} = \dfrac{T_g}{T_m}$ is approximately equal to 0.5 for a PCM in order to have a good compromise between the atomic mobilities and the driving force to form crystalline nuclei for fast recrystallisation. The information storage is based on the electrical resistance differences between the two phases. Reading is achieved by measuring the resistance using a low intensity current pulse which does not affect the state of the PCM. Switching and reading can also be carried out with the help of a laser beam for optical data storage. In this case, a pronounced difference between the optical properties of the two phases is needed (ref. 2).
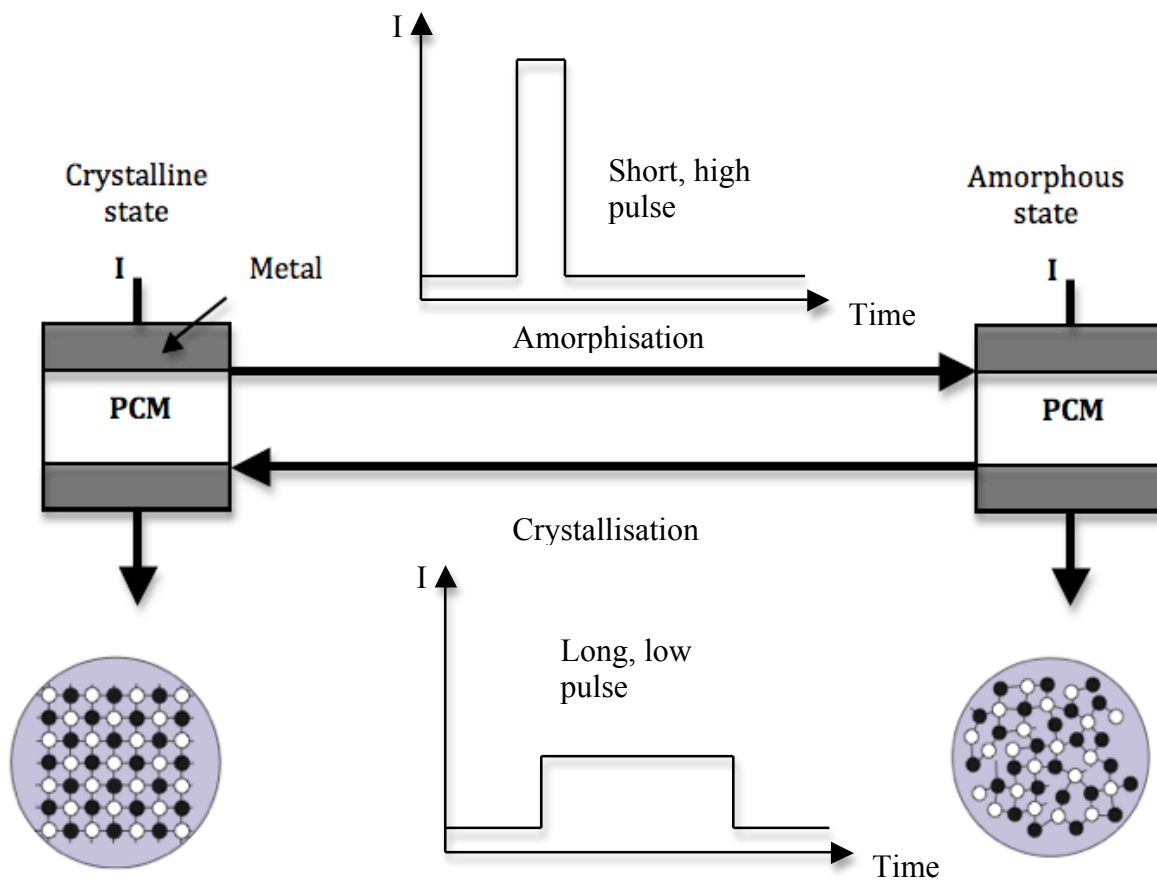

Figure 2: Switching of PCM under an electric current

1.2 Negative Thermal Expansion (NTE) in liquids

Alloys located around the eutectic composition $Ge_{15}Te_{85}$ of the binary Ge/Te system (ref. 3), exhibit a remarkable behaviour. Indeed, the volume decreases with increasing temperature in the liquid state above the melting point in a range of 100 K and then it starts to increase again as a normal liquid would do (ref. 4, see Figure 3). This decrease in specific volume when the temperature increases is named negative thermal expansion (NTE) in the literature. It is accompanied by significant change in properties, such as a sharp maximum in the constant pressure heat capacity and an increase in electrical conductivity of three orders of magnitude (ref. 5) when the temperature increases. The origin of these evolutions in the liquid state is still not well understood but it is associated with structural changes in temperature as shown by structure studies and ab initio simulations (ref. 6). It was shown that there is a distortion of the octahedral structure around Ge atoms above the melting point. When the temperature increases in the NTE range this distortion becomes smaller (see Figure 4).

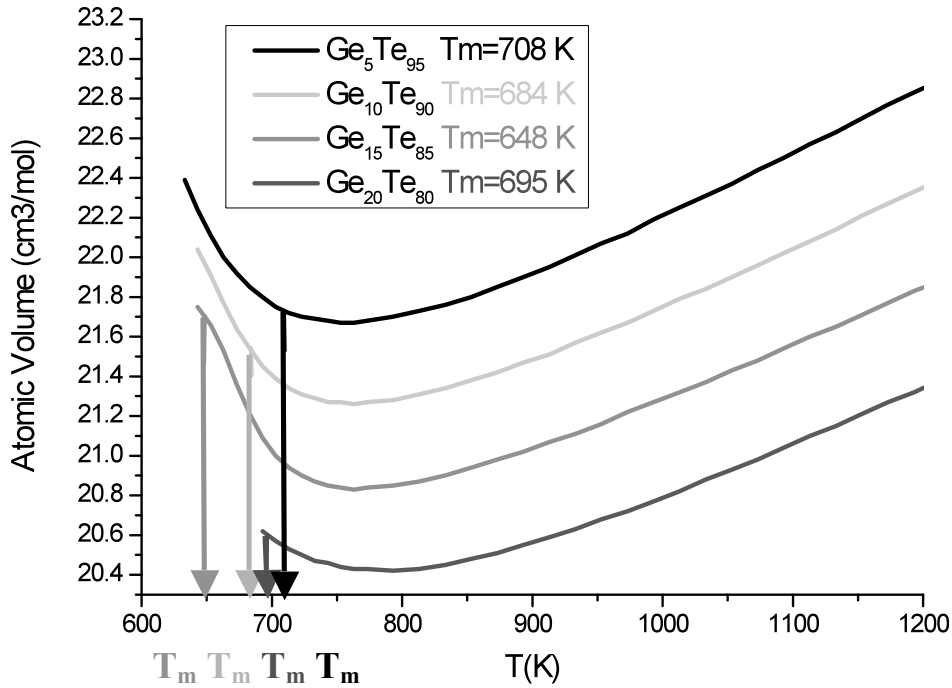**Figure 3: Volume contraction of alloys around the eutectic composition**
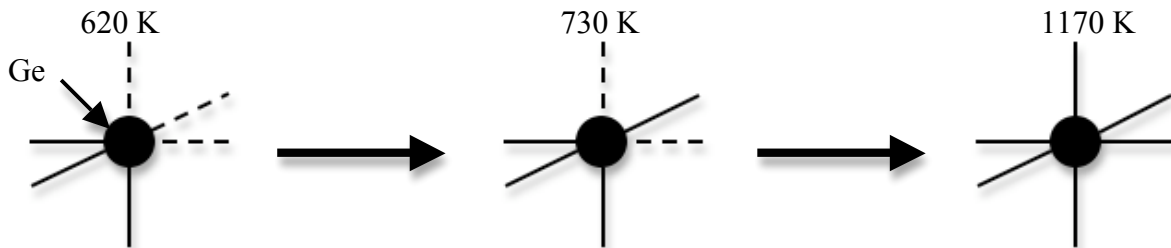

Figure 4: Evolution of the distortion around Ge atoms in $Ge_{15}Te_{85}$ in the liquid state as a function of temperature. The short bonds are represented with a solid line while the long bonds are represented with a dashed line.

3

1.3 Aim of the thesis

Contrary to $Ge_{15}Te_{85}$, it has been shown in previous studies that $Ge_{15}Sb_{85}$ does not exhibit any anomalies in the liquid state. It is then thought that, when Sb is substituted to Te, it kills off the anomalies observed in $Ge_{15}Te_{85}$. This lead to the study of the effect of substituting Te atoms by Sb, which was the subject of this thesis. Thus, $Ge_{15}(Sb_{0.1}Te_{0.9})_{85}$ and $Ge_{15}(Sb_{0.5}Te_{0.5})_{85}$ were studied. Besides, $Ge_{20}Te_{80}$ was also studied for comparison with $Ge_{15}Te_{85}$ in order to see the influence of the variation of Ge and Te concentrations on the distorted structure. On Figure 3, it can be noticed that $Ge_{20}Te_{80}$ also exhibits a NTE in the liquid state. There are well established techniques to study disordered structure. The one which was used during the master thesis is neutron scattering.

$Ge_{15}Te_{85}$ and Ge_8Te_{92} have been previously studied (ref. 7) in their liquid state during neutron scattering experiments; the results were used, in this report, for comparison.

The dynamics of $Ge_{15}Te_{85}$ in its liquid state was also studied by inelastic x-ray scattering at the European Synchrotron Radiation Facility (ESRF, Grenoble, France). A challenging sample design had to be invented for this experiment.

$Ge_{50}Te_{50}$ is known to be a PCM. It is interesting to notice that the distortion of the octahedral structure around the Ge atoms in $Ge_{15}Te_{85}$ has a direct link with what happens in the solid state for $Ge_{50}Te_{50}$, during the transition at 690 K, between the two crystalline phases α-GeTe (distorted) and β-GeTe (non-distorted). Indeed, there is a common point between the liquid studied during this master thesis and PCMs. In both cases, there is a close relation between structure changes and changes in electronic properties. In fact, PCM must have an important conductivity difference between the amorphous and the crystalline phases which implies important structure differences while the liquids which exhibit a NTE, have an important change in their conductivity. Although it is necessary to have a good understanding of the amorphous structure of PCM, it is still not well-known. In fact, it is difficult to manufacture amorphous phases in large quantities. In this case, the study of a liquid has several advantages: it is available in large quantities and the disordered structure of a liquid is expected to be close to that of the amorphous phase. Furthermore, the line between $Ge_{15}Te_{85}$ and $Ge_{15}Sb_{85}$ crosses an area where there is a PCM (see Figure 1). The understanding of what happens in those liquids could help to understand the mechanisms occurring in PCM.
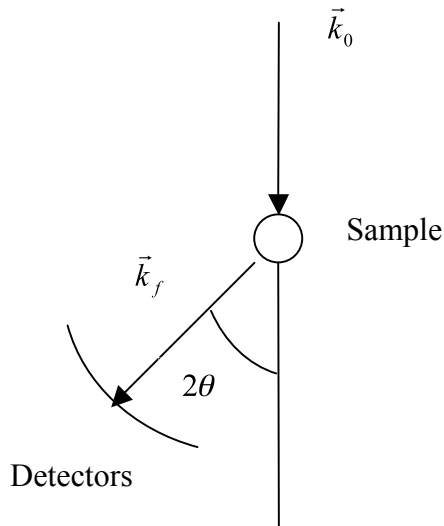
2 Formalism of Neutron Scattering

In disordered materials (liquids or amorphous), neutron scattering experiment can give information on the order of atoms at short and medium distances. This is done by the determination of the structure factor of the material which is deduced from the measurement of the scattered neutron intensity as a function of the angle.

This section, based on the article of Fisher H.E. et al. (ref. 8), describes the main equations that are necessary to understand neutron scattering.

2.1 Wave vectors scattering triangle

The sample is set under a monochromatic neutron beam. Each neutron has a momentum of $\hbar\vec{k}_0$ and energy $E_0 = \dfrac{\hbar^2 k_0^2}{2m_n}$ where m_n is the neutron mass.

- $\vec{k}_0$ is the incident wave vector of magnitude $\left\|\vec{k}_0\right\| = \dfrac{2\pi}{\lambda}$

- $\vec{k}_f$ is the final wave vector

- $\vec{Q} = \vec{k}_f - \vec{k}_0$ is the scattering vector of magnitude $Q = \dfrac{4\pi}{\lambda}\sin\theta$

The wavelength λ of a beam of neutrons used to study the atomic structure of a material is of the same order of the interatomic distances (~Å).

Figure 5: Wave vectors

2.2 Differential scattering cross section

In order to define the interaction of neutrons with matter, one defines the differential scattering cross section $\dfrac{d\sigma}{d\Omega}$ for a system of N nuclei having scattering length b_i:

$$\frac{d\sigma}{d\Omega} = \left\langle \sum_{i,j}^{N} b_i b_j e^{i\vec{Q}\cdot\vec{r}_{ij}} \right\rangle \tag{1}$$

Where, $\vec{r}_{ij} = \vec{r}_i - \vec{r}_j$ depicts the relative position between atomic sites i and j. $d\sigma$ is the number of neutrons scattered per second toward the detector into the solid angle $d\Omega$.

$\dfrac{d\sigma}{d\Omega}$ is expressed in barns/str and $1 barn = 10^{-24}$ cm^2.

The total differential cross section can be defined as $\sigma_{tot} = \int_{4\pi} \dfrac{d\sigma}{d\Omega} d\Omega$.

In reality, $\vec{r}_i$ and $\vec{r}_j$ are functions of time and scattering in liquids is an inelastic process. One should consider a double differential cross section $\dfrac{d^2\sigma}{d\Omega dE}$. In this thesis, the scattered neutrons were not analysed in energy, as a consequence, $\dfrac{d\sigma}{d\Omega}$ is given by:

$$\frac{d\sigma}{d\Omega} = \int_{-\infty}^{+\infty} \frac{d^2\sigma}{d\Omega dE} dE \tag{2}$$

The next part will present the behaviour of a monoatomic system of N atoms.

2.3   Scattering by a monoatomic system of N atoms

Even in the case of a monoatomic system, there can be more than one scattering length because each isotope of one element has its own scattering length. By considering that there is no correlation between the scattering lengths and the atom positions, equation (1) can be written as

$$\frac{d\sigma}{d\Omega} = \bar{b}^2 \left\langle \sum_{i,j}^{N} e^{i \cdot \vec{Q} \cdot \vec{r}_{ij}} \right\rangle + \sum_{i}^{N} (\overline{b^2} - \bar{b}^2) \tag{3}$$

Where, $\overline{b^2} = \langle b_i b_i \rangle$ and $\bar{b}^2 = \langle b_i b_j \rangle$, i≠j

The structure factor $S(\vec{Q})$ is defined as

$$S(\vec{Q}) = \frac{1}{N} \left\langle \sum_{i,j}^{N} e^{i \cdot \vec{Q} \cdot \vec{r}_{ij}} \right\rangle \tag{4}$$

The limit value of S(Q) is $S(Q \to \infty) = 1$ and it can be noticed that $S(Q) \geq 0$. Figure 6 shows S(Q) for systems of different nature.
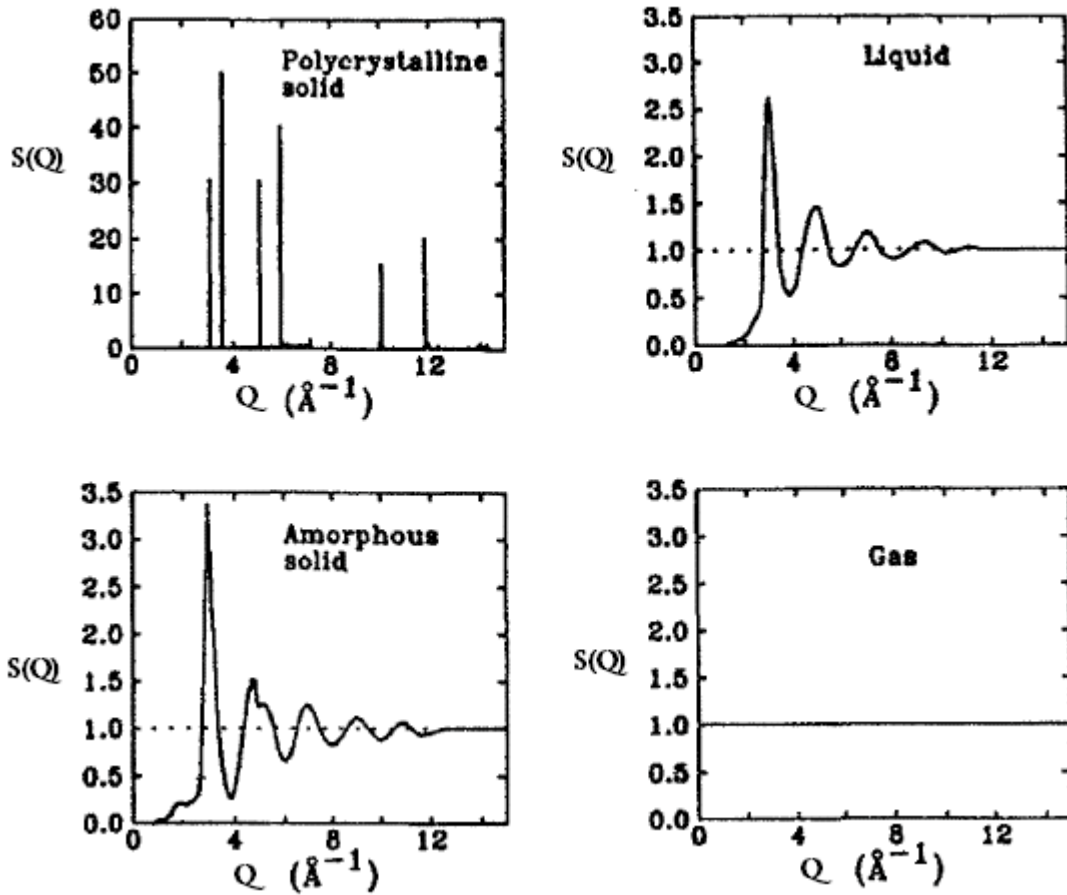
Figure 6: Structure factors for different systems

From equation (3), it can be deduced:

$$\frac{1}{N}\frac{d\sigma}{d\Omega}(\vec{Q}) = \bar{b}^2 S(\vec{Q}) + (\overline{b^2} - \bar{b}^2)$$

(5)

Which is often written as $b_{coh}^2 S(\vec{Q}) + b_{incoh}^2$

Equation (5) shows clearly that $\frac{d\sigma}{d\Omega}$ is divided into two terms; a coherent one relative to the scattering by atoms with the same scattering length $\bar{b}$ and an incoherent one (independent of $\vec{Q}$) which is the consequence of the random distribution of isotopes and hence scattering length. b_{coh} is simply the average of the scattering lengths distribution on all the isotopes in the sample. b_{incoh} is the variance of that distribution. In a liquid, scattering does not depend on the direction and then Q does not have to be considered as a vector.

It can be noticed that $\frac{1}{N}\frac{d\sigma}{d\Omega}(Q \to \infty) = \bar{b}^2 S(Q \to \infty) + (\overline{b^2} - \bar{b}^2) = \bar{b}^2 * 1 + (\overline{b^2} - \bar{b}^2) = \overline{b^2}$.

The values of the parameters b_{coh}, b_{incoh} or σ_{coh} and σ_{incoh} are determined experimentally and can be found in the literature for each element (ref. 9).

In order to represent, the atomic structure of a sample, a new function is defined which is the atomic pair distribution function g(r). Let's consider the probability of finding an atom at a distance r from an atom defined as the origin. g(r) is an average of this probability on all the origins possible and it gives an information on the interatomic distances typically in the range from 0 to 15 Å.

S(Q) and g(r) are linked by a Fourier transform.

$$S(Q) - 1 = \frac{4\pi\rho_0}{Q} \int r[g(r) - 1]\sin(Qr)dr$$

$$g(r) - 1 = \frac{1}{2\pi^2\rho_0 r} \int Q[S(Q) - 1]\sin(Qr)dQ$$

(6)

Where ρ_0 is the atom density.

Another useful function is the Radial Distribution Function RDF(r):

$$RDF(r) = 4\pi r^2 \rho_0 g(r)$$

(7)

By integrating this function one can obtain the number of atoms between two spheres of radii r_1 and r_2:

$$\bar{n} = \int_{r1}^{r2} RDF(r)dr$$

(8)

In order to have an estimation of the coordination number, r_1 and r_2 have to be chosen properly. r_1 and r_2 are two consecutives minima of the RDF(r) function (see Figure 7).
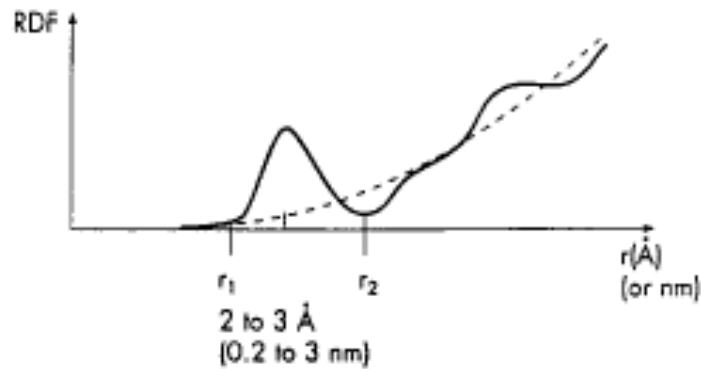

Figure 7 : Radial Distribution Function RDF(r)

2.4 Scattering by a polyatomic system of n atomic species

The approximation that there is no correlation between the scattering lengths and the atom positions that was made for a monoatomic system is not valid for polyatomic systems where there are correlations. In this case, partial structure factors for the different atomic systems have to be defined.

The total structure factor can be written

$$S_T(Q) = \frac{1}{\bar{b}^2} \sum_{\alpha,\beta}^{n} c_\alpha c_\beta \bar{b}_\alpha \bar{b}_\beta S_{\alpha\beta}(Q) \tag{9}$$

where $S_{\alpha\beta}(Q)$ is the partial structure factor of atomic species α and β, c_α is the concentration of α such as $\sum_{\alpha}^{n} c_\alpha = 1$, $\bar{b} = \sum_{\alpha}^{n} c_\alpha \bar{b}_\alpha$ and $\overline{b^2} = \sum_{\alpha}^{n} c_\alpha \overline{b_\alpha^2}$.

$S_{\alpha\beta}(Q)$ is linked with the partial pair distribution functions by Fourier transform:

$$S_{\alpha\beta}(Q) - 1 = \frac{4\pi\rho_0}{Q} \int_0^\infty r\left[g_{\alpha\beta}(r) - 1\right]\sin(qr)dr$$

$$g_{\alpha\beta}(r) - 1 = \frac{1}{2\pi^2 r\rho_0} \int_0^\infty Q\left[S_{\alpha\beta}(Q) - 1\right]\sin(qr)dQ \tag{10}$$

The general form of equation (5) is:

$$\frac{1}{N}\frac{d\sigma}{d\Omega}(Q) = \bar{b}^2 S_T(Q) + (\overline{b^2} - \bar{b}^2) \tag{11}$$

As for a monoatomic system, it can be noticed that the incoherent term is the variance of the scattering length distribution.

During an experiment, $S_T(Q)$ is obtained and not the $S_{\alpha\beta}(Q)$. A Fourier Transform of $S_T(Q)$ calculated from equation (6) gives an expression of the total pair distribution function:

$$g_T(r) = \frac{1}{\bar{b}^2} \sum_{\alpha,\beta}^{n} c_\alpha c_\beta \bar{b}_\alpha \bar{b}_\beta g_{\alpha\beta}(r) \tag{12}$$

$g_T(r)$ gives an information on the interatomic distances balanced with the scattering lengths. The neutron scattering experiment will provide the total structure factor of a material. The partial structure factors can be obtained by ab-initio calculations. Those factors give access to information on each element. For instance one could obtain the coordination number for each element in the system.

3   Experimental Aspects

3.1   The spectrometer

Experiments were performed at the 'Laboratoire Léon Brillouin' (LLB) at CEA (Atomic Energy Centre) Saclay, France. The spectrometer used (7C2) was a hot neutron two-axis diffractometer (Figure 8).
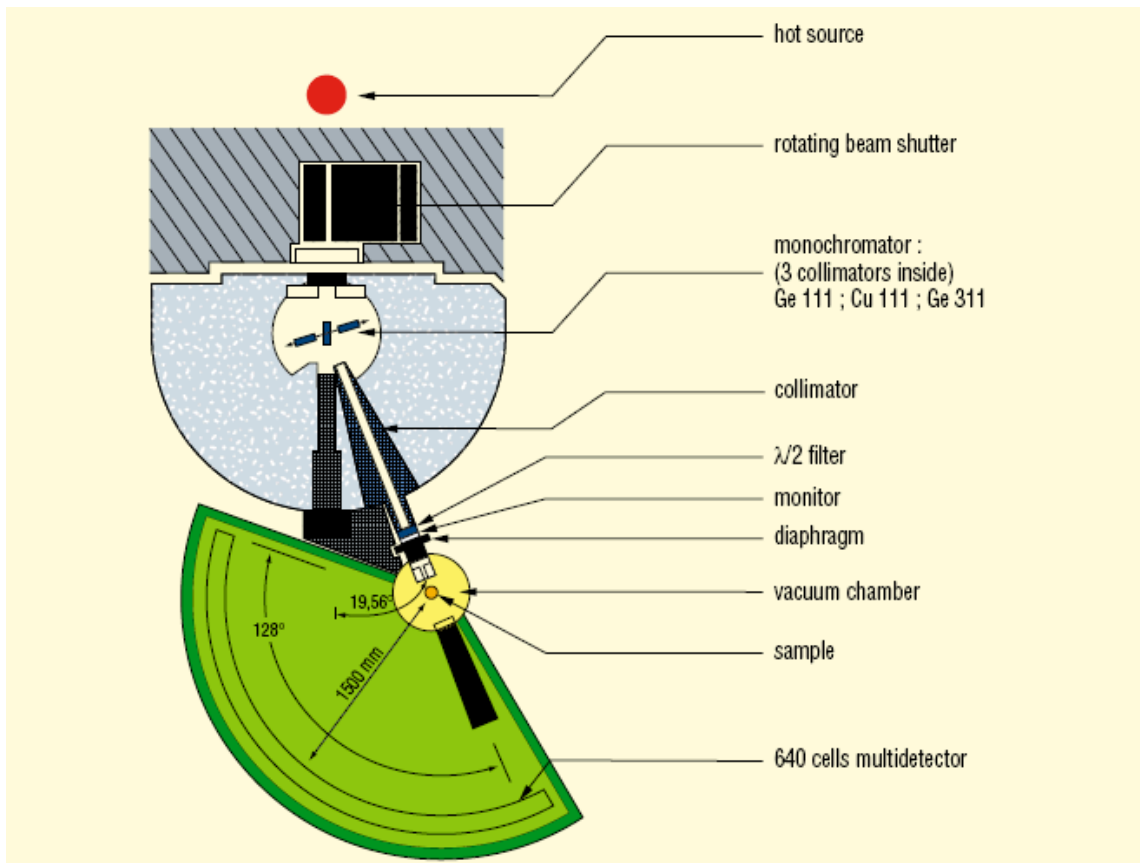

Figure 8 : General layout of the hot neutron two-axis diffractometer 7C2 (http://www-llb.cea.fr/)

The function of the rotating beam shutter is to stop the arrival of neutrons when a modification of the monochromators is required but the shutter is always open in operation. The monochromator selects the required wavelength. The collimator reduces the divergence. Two diaphragms (one horizontal and one vertical) give appropriate dimensions (adapted to the sample) to the neutron beam (the beam used was 5cm high and 1cm wide).
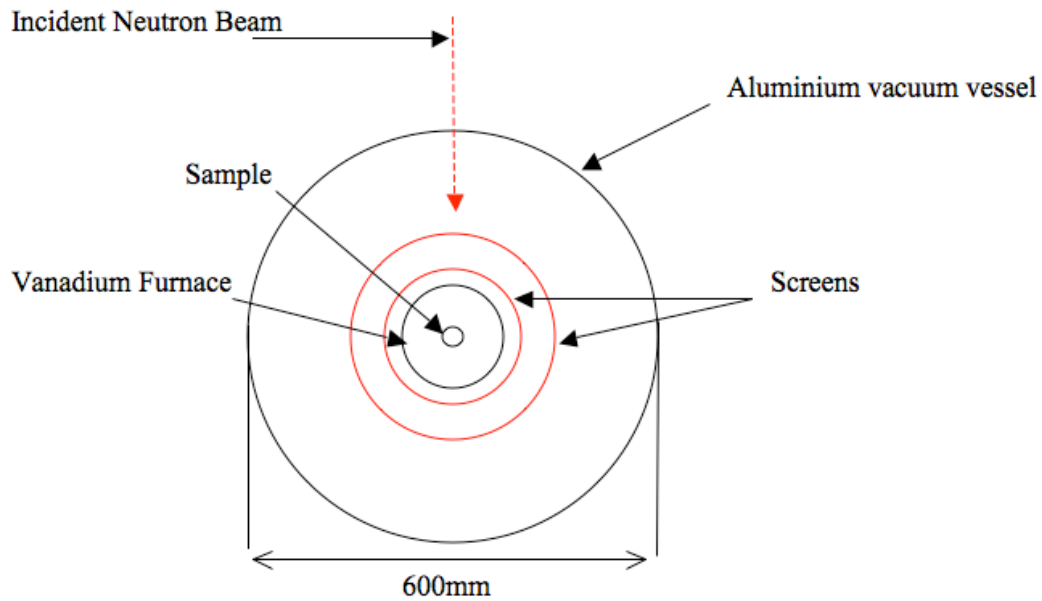
The sample is placed in a vacuum vessel to avoid neutron diffusion by air. The sample is surrounded by a furnace fabricated from a foil of vanadium (100 μm thick). There are two thermocouples at the bottom of the sample to regulate and measure the sample temperature and two screens between the furnace and the vessel that prevent the chamber being warmed up by the heat from the furnace (see Figure 9). A vacuum also prevents the furnace from being oxidized and avoids heat conduction between the furnace and the vacuum vessel. A vacuum is created using two pumps. A primary pump creates a vacuum to a pressure of

10^{-3} bars and a turbo pump reduces the pressure further, to about 10^{-5} bars. The furnace can only be warmed up if the pressure is below 10^{-5} bars.

During a neutron scattering experiment, the number of neutrons arriving per second on one detector (solid angle $d\Omega$) is measured and is given by:

$$I(Q) = \Phi \frac{d\sigma}{d\Omega} d\Omega \qquad (13)$$

Where, Φ (s^{-1} cm^{-2}) is the incident neutron beam flux

Figure 9 : Vacuum vessel

The neutron beam is scattered towards 640 detectors equally distributed, every 0.2°, over 128°. The 'banana' of detectors is surrounded by a polyethylene protection. The sample to detector distance is 1.5m.

The wavelength of the experiment was $\lambda = 0.724$ Å.

3.2   Hot source principle

When they go out of the reactor, the neutrons have a high kinetic energy which has to be reduced. To do so, they are thermalised by interacting with a medium maintained at a fixed temperature, a hot source at a temperature of 1400K in the case of 7C2.

The kinetic energy of neutrons can be expressed by two expressions:

❖ The classic physics relationship that describes the kinetic energy $K_E = \left\langle \frac{1}{2} m_n v^2 \right\rangle$ where m_n is the mass of the neutron and v its velocity.
❖ The relationship that relates the average kinetic energy of a moving molecule and temperature $K_E = \left\langle \frac{3}{2} k_B T \right\rangle$ where $k_B = 1.381*10^{-23}$ J/K is the Boltzmann constant.

If these two relationships are equated, it gives: $\left\langle \frac{1}{2} m v^2 \right\rangle = \left\langle \frac{3}{2} k_B T \right\rangle$. From this equation, it can be seen that the kinetic energy and thereby the velocity of neutrons can be reduced by reducing temperature.

3.3   The samples

The samples used during these experiments were $Ge_{15}(Te_{0.9}Sb_{0.1})_{85}$, $Ge_{15}(Te_{0.5}Sb_{0.5})_{85}$ and $Ge_{20}Te_{80}$. They have been studied in the liquid state at different temperatures. Prior to the experiment, the samples were sealed in an amorphous SiO2 quartz tube (inner diameter 8mm, outer diameter 10mm) under vacuum.

4   Data Analysis

It is necessary to make the right corrections to the measured spectrum by subtracting the scattered intensities coming from the sample container, the sample environment and the background. The multiple scattering phenomenon, as well as inelastic corrections, must also be considered. After these corrections, one obtains the interatomic pair distribution function by a Fourier transform of the structure factor. Performing this experiment at different temperatures in the liquid state gives an idea of the change occurring in the structure by analyzing, for example, the evolution of the coordination numbers deduced from the pair distribution function. The corrections to be applied to obtain the structure factor are similar for every sample so only the results from the $Ge_{20}Te_{80}$ experiments will be detailed in this section. $Ge_{20}Te_{80}$ has a melting temperature of 700 K (ref. 3). During the experiment, the temperature is increased gradually until the sample melts; that is to say when the Bragg peaks disappear. There are no more Bragg peaks when 723 K is reached, which is an approximation of the experimental melting point. The measurement temperatures (850 K, 733 K and 973 K) are chosen from Figure 3 in order to be in the NTE (Negative Thermal Expansion) range. The sample is kept for 11 hours at each temperature in order to give enough statistics. The same process is performed on the empty quartz tube at temperatures of 733 K and 973 K during similar times. The empty vacuum vessel signal is independent of temperature and it has been measured. In the following section the method for obtaining the static structure factor S(Q) from the measured intensity for the temperature of 850 K is detailed.

4.1   Detector efficiency correction

Each detector has a given efficiency, e. In order to measure the efficiency of the detectors, a sample of vanadium with the same dimensions as the sample is measured. The vanadium is used because its signal is incoherent and as a consequence it is not dependent upon Q which is necessary to calibrate. Figure 10 shows the measured efficiency of the 640 detectors.
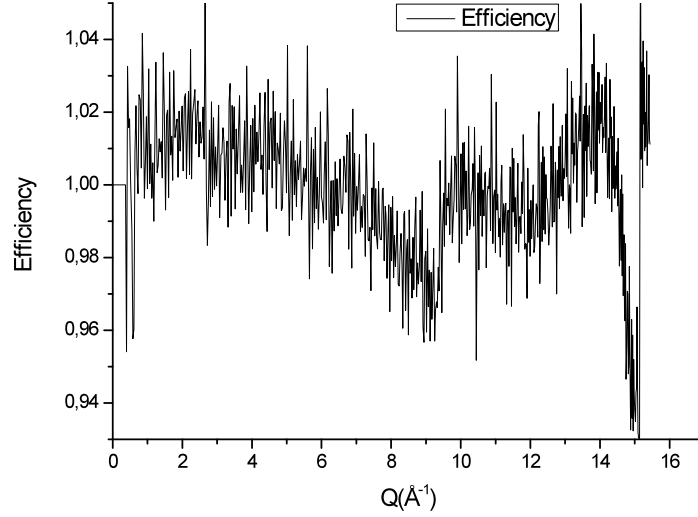

Figure 10 : Detectors efficiencies

The measured intensity I_{s0} from the sample is divided by the previous signal to obtain the "real" measured intensity I_{s1}.

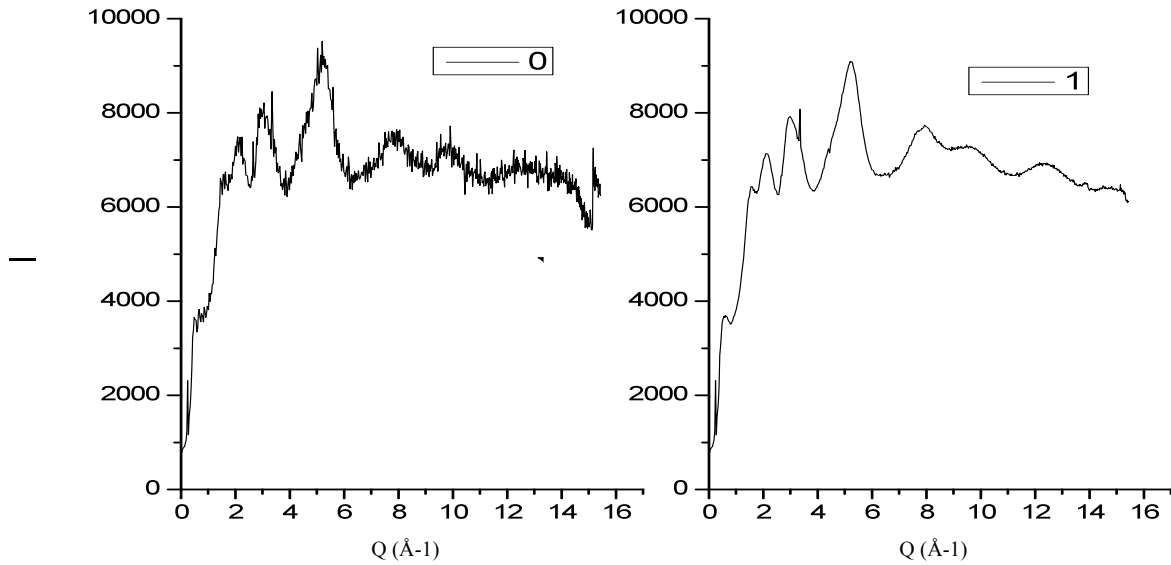$$I_{s1} = \frac{I_{s0}}{e} \tag{14}$$

Figure 11 : On the left, the original measured intensity from the sample and on the right, the spectrum corrected from the efficiency of the detector

The drop of $I_{s1}(q)$ for q>14.5 Å^{-1} is mainly due to a problem with the efficiency of some detectors which could not be corrected.

4.2   Vacuum vessel correction

The signal from the vacuum vessel I_v is measured without the furnace or a sample at room temperature as it is temperature independent. It is then subtracted from the original intensity to obtain the intensity from the sample I_{s2}.
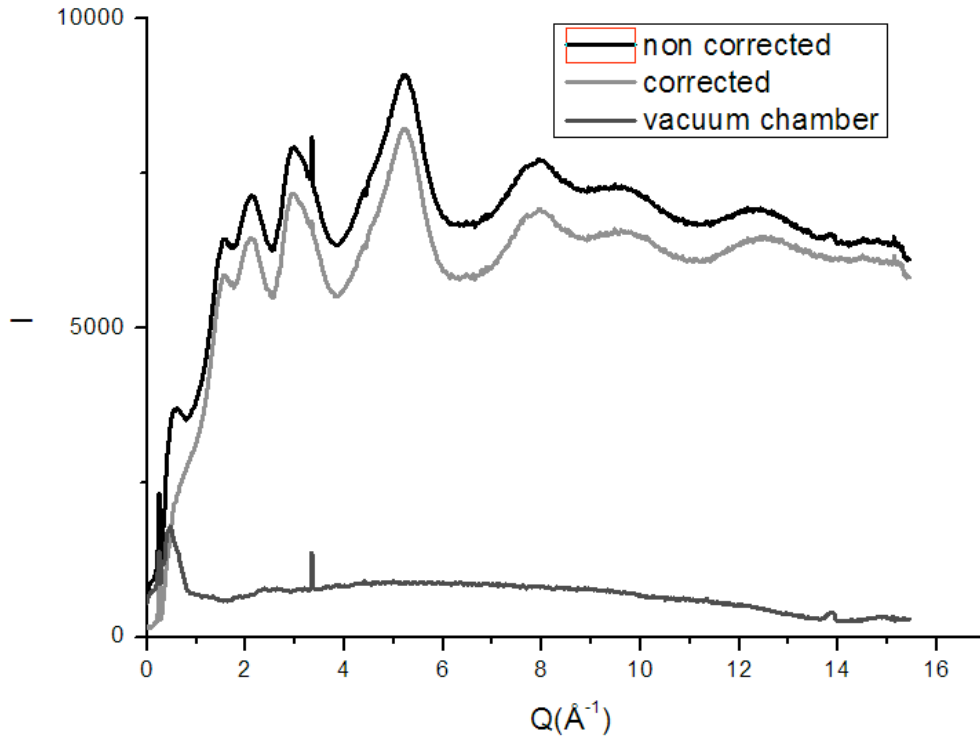
$$I_{s2} = I_{s1} - I_v \tag{15}$$

Figure 12 : Vacuum vessel correction, for Ge$_{20}$Te$_{80}$ at 850 K

The signal from the empty vacuum vessel is almost a flat signal.

4.3   Quartz correction and self absorption

The signal measured from the empty quartz at 850K is interpolated from the two signals at 733 K and 973 K.

When measuring the sample, the signal of the quartz is affected due to the absorption and the scattering of neutrons by the sample. This problem has been tackled by Paalman and Pings (ref. 10). The corrected intensity from the sample is given by:
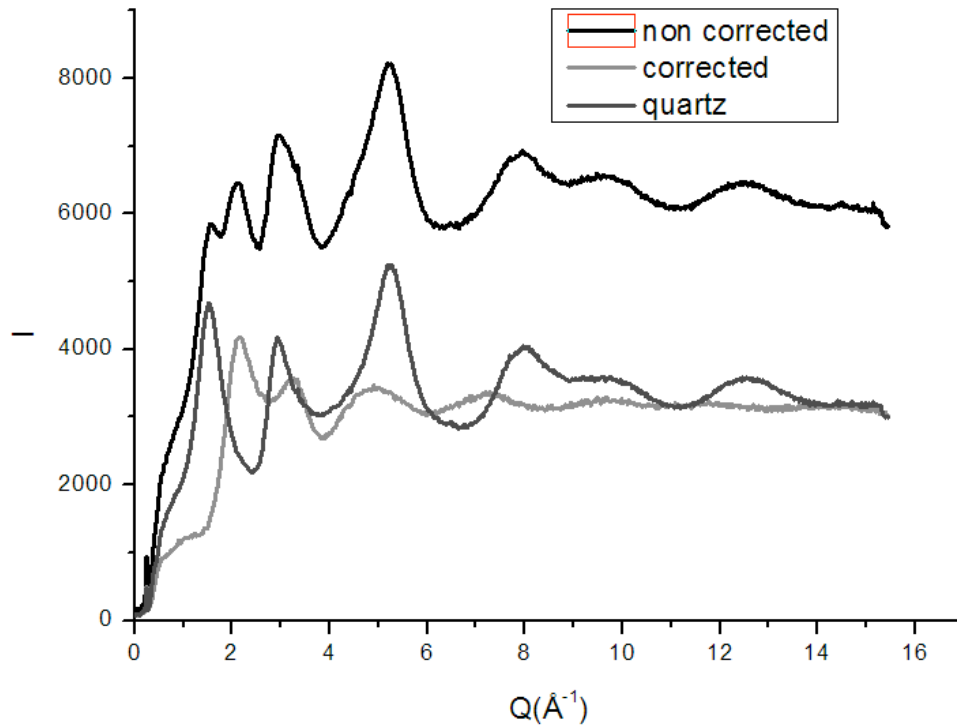
$$I_{s4} = \beta(\theta) \times (I_{s3})$$
$$\text{Where } I_{s3} = I_{s2} - \alpha(\theta)I_{empty}$$

(16)

Where I_{empty}, is the measured intensity of the quartz tube alone, $\alpha(\theta)$ (~1) is the percentage of the quartz signal to remove and $\beta(\theta)$ (>1) characterises the self absorption effect.

The coefficient $\alpha(\theta)$ and $\beta(\theta)$ are calculated using programs which carry out the integration for a filled cylindrical sample of radius R_{int} and its cylindrical container of internal radius R_{int} and external radius R_{ext}. The absorption coefficients of the sample and the container are needed to run the programs (Appendix 3).

Figure 13 shows the application of the following correction $I_{s3} = I_{s2} - \alpha(\theta)I_{empty}$.

Figure 13: Quartz correction, for Ge$_{20}$Te$_{80}$ at 850 K

The signal of the quartz is of the same order of magnitude of the total signal hence it must be counted for the same duration in order to give enough statistics.

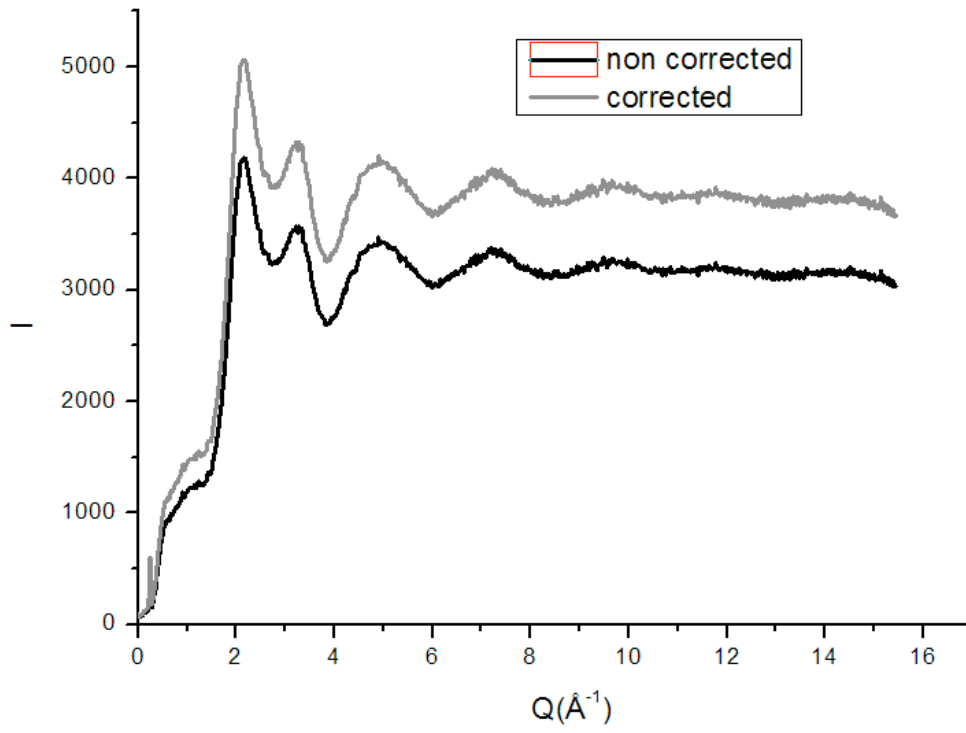Figure 14 shows the application of the correction $I_{s4} = \beta(\theta)I_{s3}$.

Figure 14: Self absorption correction, for Ge$_{20}$Te$_{80}$ at 850 K

4.4   Multiple scattering correction

A given neutron can be scattered several times due to the high number of atoms. The multiple scattering contributes to the measured signal and must be substracted in order to keep only the signal from simple scattering processes. Blech and Averback (ref. 11) suggested a way to correct multiple scattering, considering that it is an isotropic phenomenon and that the probability to have another scattering is a constant: $I_n / I_{n-1} = \delta'$. The intensity after n successive scattering events, I_n, is a geometric series hence its sum is, $I_{mult} = \langle I_1 \rangle (\delta' / [1 - \delta'])$ where $\langle I_1 \rangle$ is the average intensity of simple scattering processes only.

As a consequence, the measured signal, I_{meas}, is given by $I_{meas} = I_1 + I_{mult}$.
After simple calculations it can be observed that

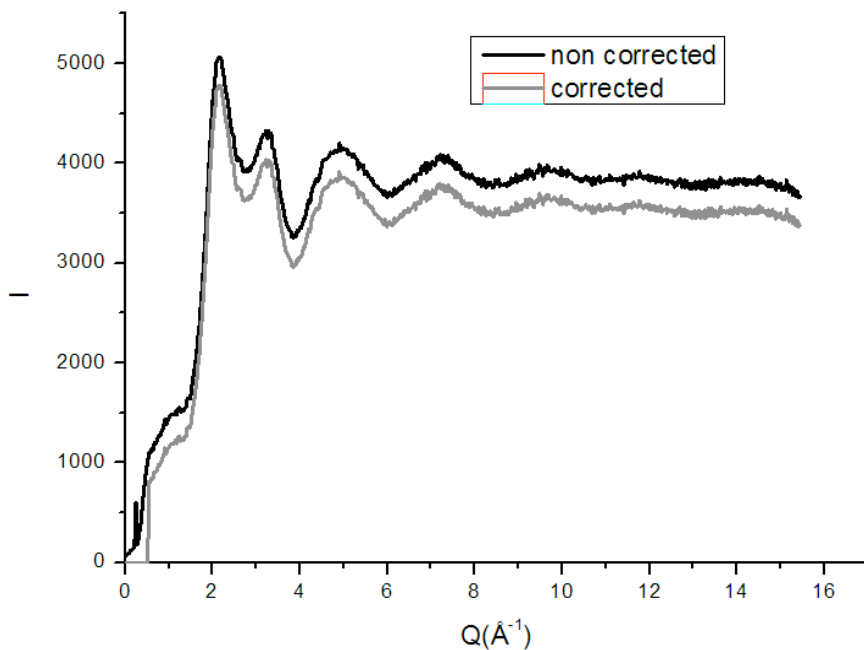$$I_1 = I_{meas} - \delta' \langle I_{meas} \rangle \qquad (17)$$

where δ' is the percentage of multiple scattering in I_{meas}.
δ' can be defined as a function of the scattering and absorption cross sections σ_{scatt} and σ_{abs} (Appendix 2):

$$\delta' = \frac{\sigma_{scatt}}{\sigma_{tot}} \delta \qquad (18)$$

where σ_{scatt} is the scattering cross section, σ_{tot} is the total cross section and δ is a constant that depends only upon the geometrical characteristics of the cylindrical sample.
Figure 15 shows the signal before and after the multiple scattering correction.

Figure 15 : Intensity of the signal before and after subtracting the multiple scattering effect, for Ge$_{20}$Te$_{80}$ at 850 K

4.5   Inelastic correction (Placzeck correction)

In the static approximation, Q, is linked to 2θ by the equation $Q = \dfrac{4\pi}{\lambda_0}\sin\theta$. However, Q is significantly dependent upon the energy E at a given 2θ. The energy variation at each angle is not taken into account by the detectors. Placzeck (ref. 12) was the first to suggest a correction that would re-establish the signal as it would be by considering this variation. Figure 16 illustrates this correction.
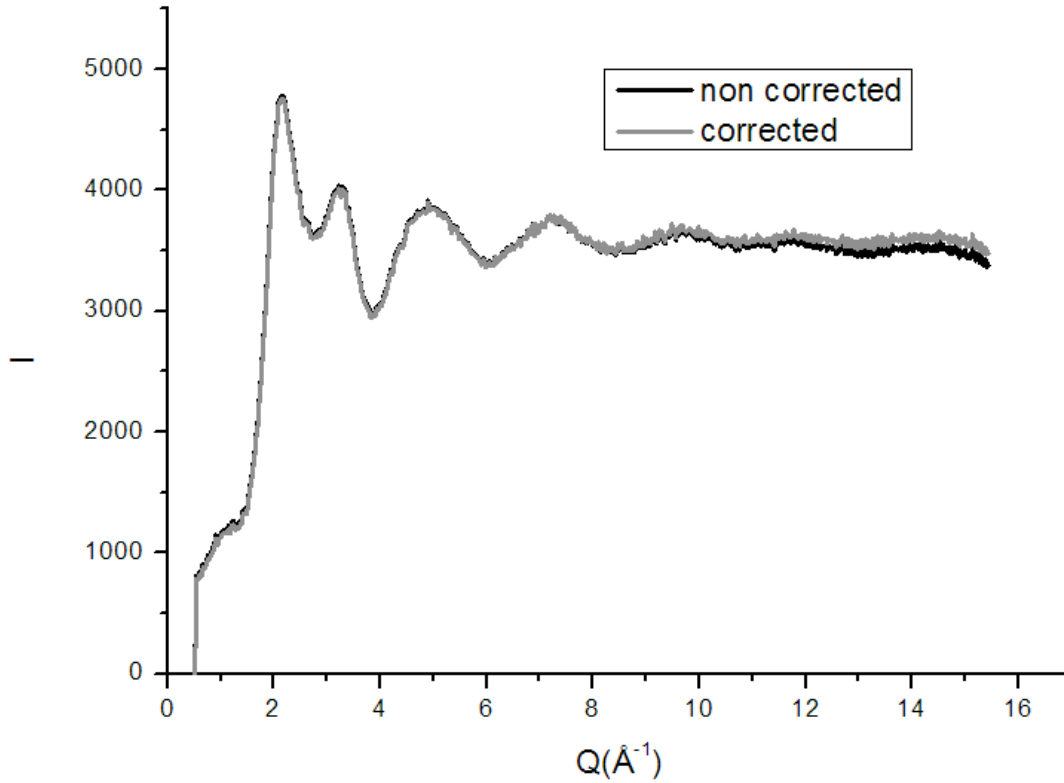

Figure 16 : Placzeck correction, for Ge$_{20}$Te$_{80}$ at 850 K

The effect of this correction is more important at high Q. The asymptotic value rises by 3%, which shows that this correction cannot be neglected even if it is less important than the previous ones.

When this last correction is done, the signal has to be normalized in order to tend toward 1 because $S(Q \to \infty) = 1$.

From equation (5), it can be deduced that $\dfrac{d\sigma}{d\Omega}(Q \to \infty) = \overline{b}^2 * 1 + (\overline{b^2} - \overline{b}^2) = \overline{b^2}$. In the case of Ge$_{20}Te_{80}$, $\overline{b}^2 = 0.412$ and $\overline{b^2} = 0.394$ (see Appendix 2). The operation to make the spectrum tend towards $\overline{b}^2$ is:

$$\frac{d\sigma}{d\Omega}(T = 577°C) = \frac{I_{s6} * \overline{b^2}}{I_\infty} \tag{19}$$
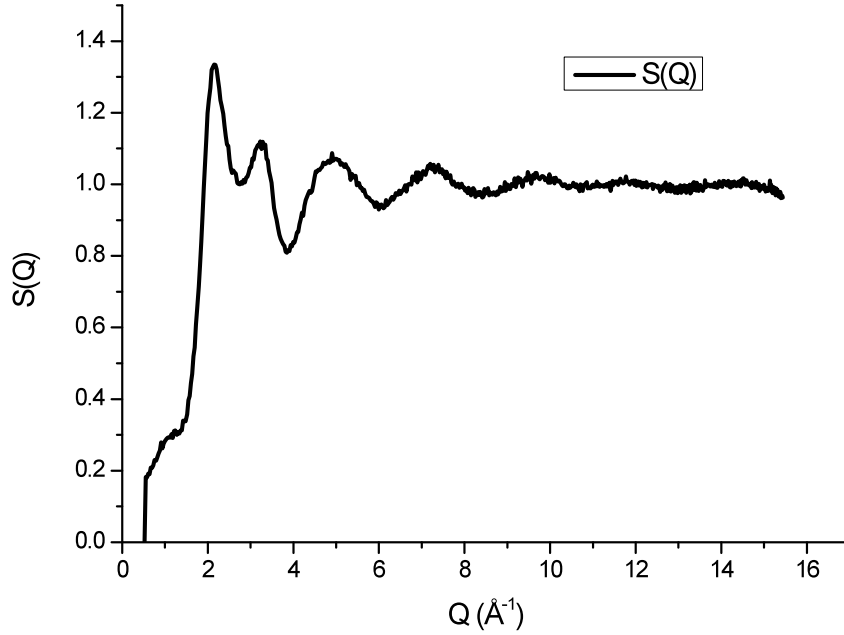
Where I_∞ is the asymptotic value of the spectrum I_{s6}.

20

From equation (5), it can then be deduced that:

$$S(Q) = \frac{d\sigma}{d\Omega} * \frac{1}{\overline{b}^2} - \frac{\overline{b^2}}{\overline{b}^2} + 1 \qquad (20)$$

As a consequence, $S(Q, T = 577°C) = \dfrac{\dfrac{d\sigma}{d\Omega}(T = 577°C)}{0.394} - \dfrac{0.412}{0.394} + 1$. Figure 17 shows the final structure factor S(Q) of $Ge_{20}Te_{80}$ at T=850 K after application of all of the corrections.

Figure 17: Structure factor S(Q) of $Ge_{20}Te_{80}$ at T=850 K after all corrections made

The same procedure must be repeated for each composition (see 3.3) and each temperature.

4.6   Pair distribution function

In order to perform the Fourier transform of equation (6), different parameters have to be considered. First, the structure factor has to strictly tend toward 1 so the data after Q=15 Å^{-1} will not be considered due to the sudden anomalous decrease of the structure factor in this area due to the detectors (see 4.1). Then, it is necessary to choose a suitable cut-off function in order to limit the cut-off oscillations on the g(r). The retained function is:

$$f(Q) = \frac{\sin(Q * \frac{\pi}{Q_{cut}})}{Q * \frac{\pi}{Q_{cut}}} \qquad (21)$$

with Q_{cut}=15 Å^{-1}.

Considering this function, g(r) is given by:

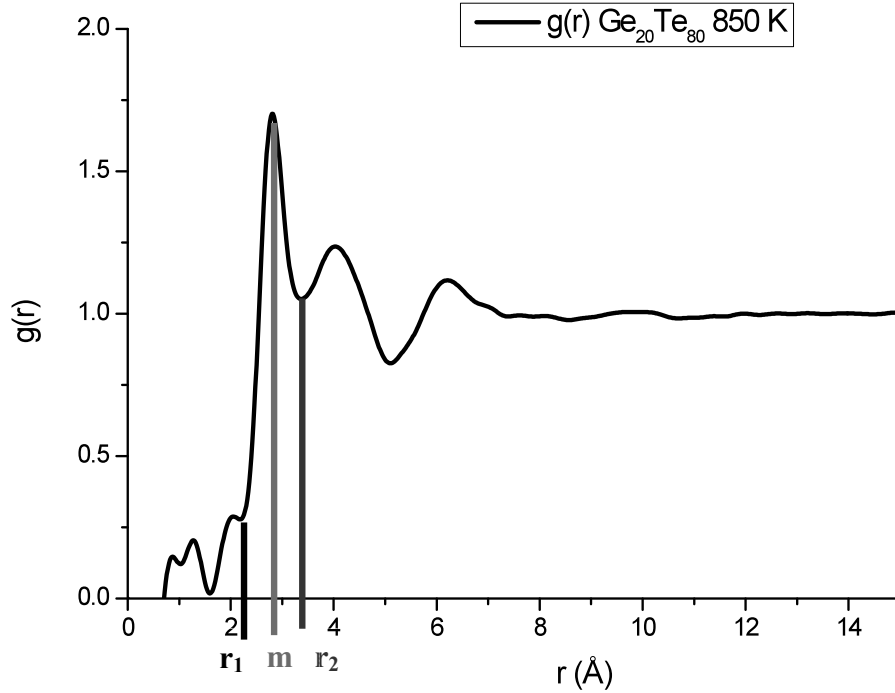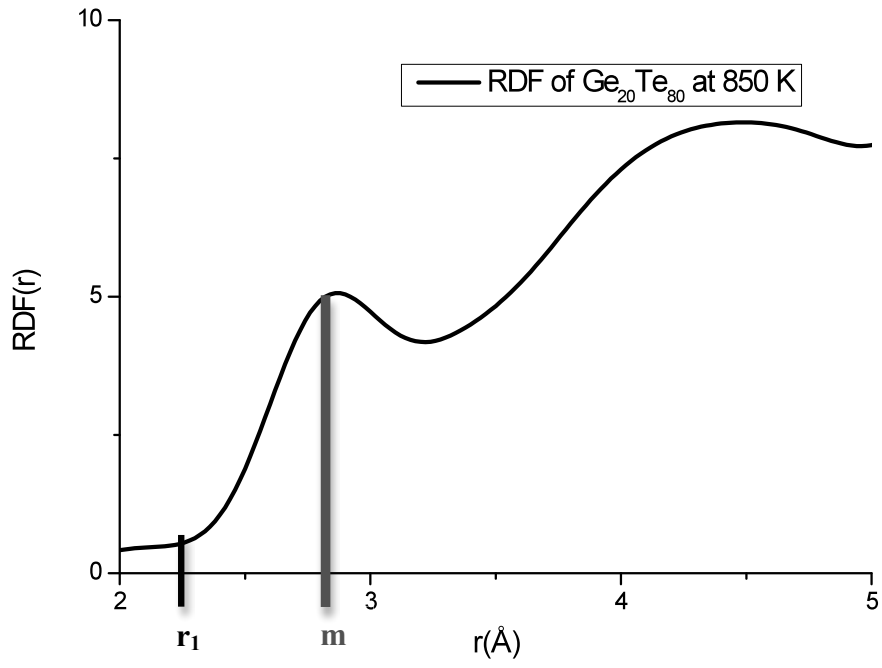$$g(r) = 1 + \frac{1}{2\pi^2 r \rho_0} \int_0^\infty Q(S(Q) - 1)\sin(Qr)dQ \qquad (22)$$

Figure 18: Atomic pair distribution of Ge$_{20}$Te$_{80}$ at 850 K

The average coordination number of all the atoms can be calculated by integrating the radial distribution function (equation (8)) between r_1 and r_2 (see Figure 18). Although r_1 is well defined, an uncertainty exists on where to take r_2. As the first peak is symmetrical, integration between r_1 and the maximum of the first peak multiply by 2 will give a correct estimation of the coordination number.
The radial distribution function is represented on Figure 19.

Figure 19: Radial Distribution Function RDF(r) of Ge$_{20}$Te$_{80}$ at 850 K

The result of the integral between r$_1$=2.26 and m=2.8 is $\bar{n} = 2 * \int_{r1}^{m} RDF(r)dr$ which tells us that the average coordination number is $\bar{n} = 2.14$ for Ge$_{20}$Te$_{80}$ at 850 K.

5 Results

5.1 The structure factors

The structure factors of all the studied samples are represented in this section.
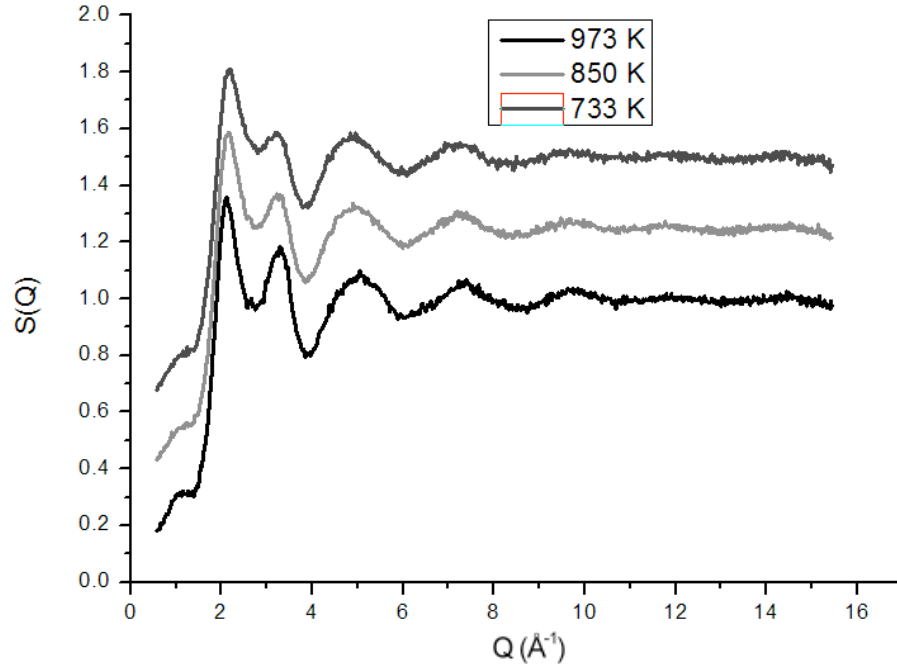
5.1.1 $Ge_{20}Te_{80}$

Figure 20: Structure factor of $Ge_{20}Te_{80}$ at 3 temperatures T= 733 K, 850 K and 973 K (the curves were shifted, in order to separate them)
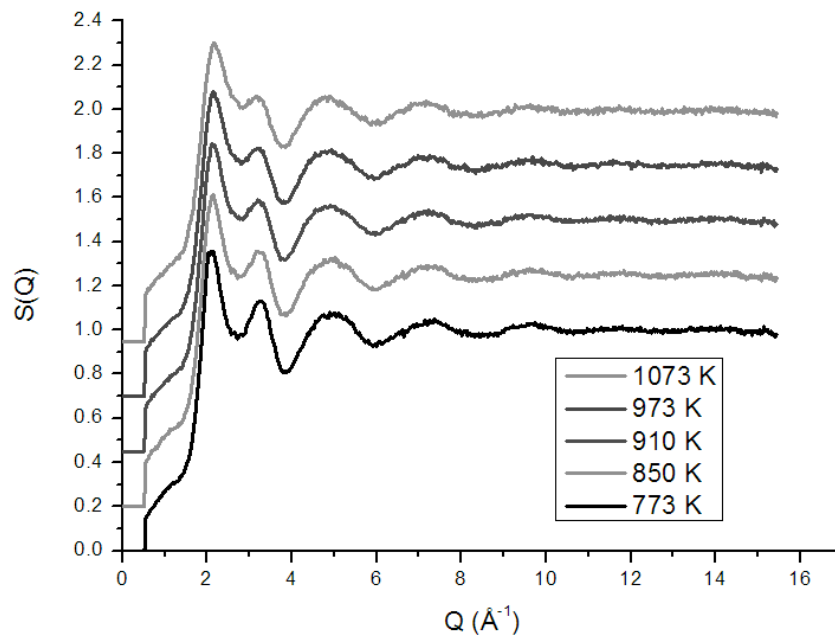
5.1.2 $Ge_{15}(Sb_{0.1}Te_{0.9})_{85}$

Figure 21: Structure factors of $Ge_{15}(Te_{0.9}Sb_{0.1})_{85}$ at 5 temperatures, T=773 K, 850 K, 910 K, 973 K ,1073 K
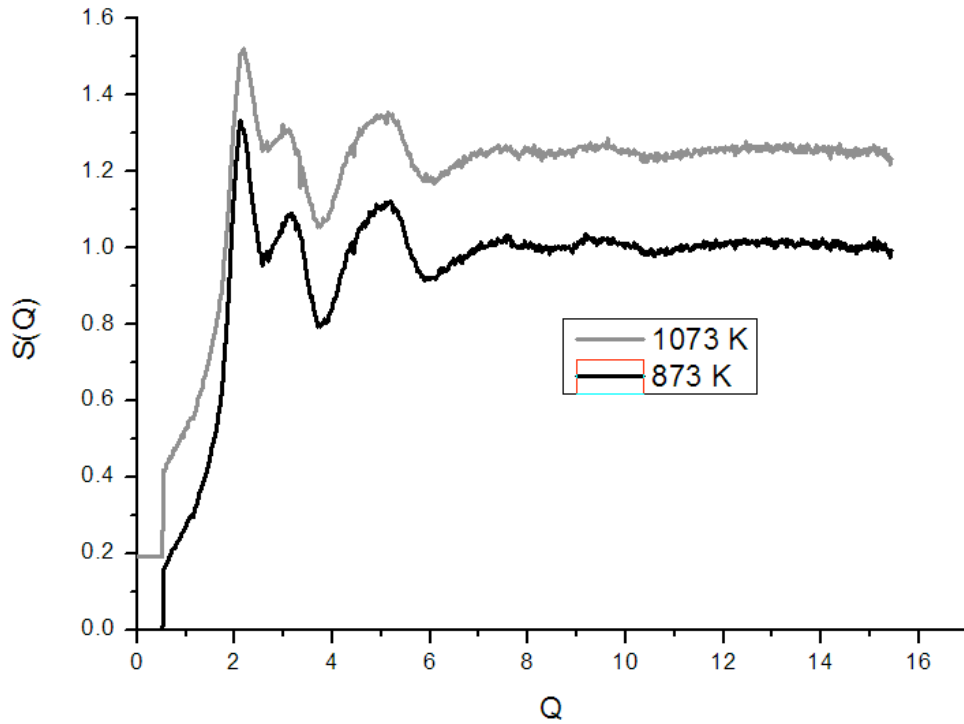
5.1.3 $Ge_{15}(Sb_{0.5}Te_{0.5})_{85}$

Figure 22: Structure factors of $Ge_{15}(Te_{0.5}Sb_{0.5})_{85}$ at 2 temperatures, T=873 K and 1073 K

5.1.4 General observations on the structure factors

The structure factors of $Ge_{15}Sb_{85}$ and Ge_8Te_{92} have been obtained during previous studies (Appendix 4). Some observations can be made about the evolution of the structure factors with the temperature for the different compositions. Without regarding the composition, it can be noticed that the two first peaks of the S(Q) evolve with temperature (the first one decreases while the second one increases when temperature increases). When substituting Sb to Te in $Ge_{15}Te_{85}$, this evolution is reduced. Thus, for $Ge_{15}Sb_{85}$ there are almost no changes of the structure factor when the temperature increases. This is a proof that there are structural differences between $Ge_{15}Te_{85}$ and $Ge_{15}Sb_{85}$ as they do not behave in the same way at similar temperatures.

Figure 23 shows the evolution in temperature of the structure factor of $Ge_{15}Te_{85}$. A pre-peak can be noticed for the lower temperatures and it has totally disappeared at 796 K. This pre-peak is thought to be the result of the distorted structure and it disappears when the structure becomes more symmetric.

Figure 24 shows the structure factors for four alloys along the line between $Ge_{15}Te_{85}$ and $Ge_{15}Sb_{85}$ (Figure 1) for temperatures just above the liquidus. It can be noticed that the pre-peak is no longer observable when adding some Sb.
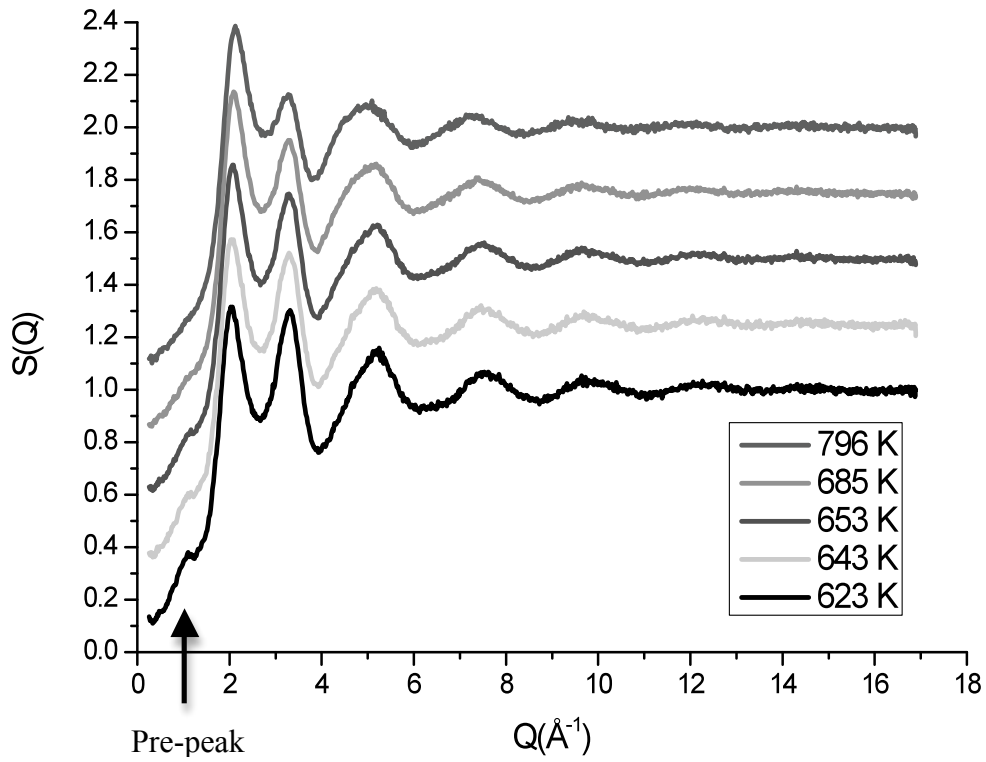
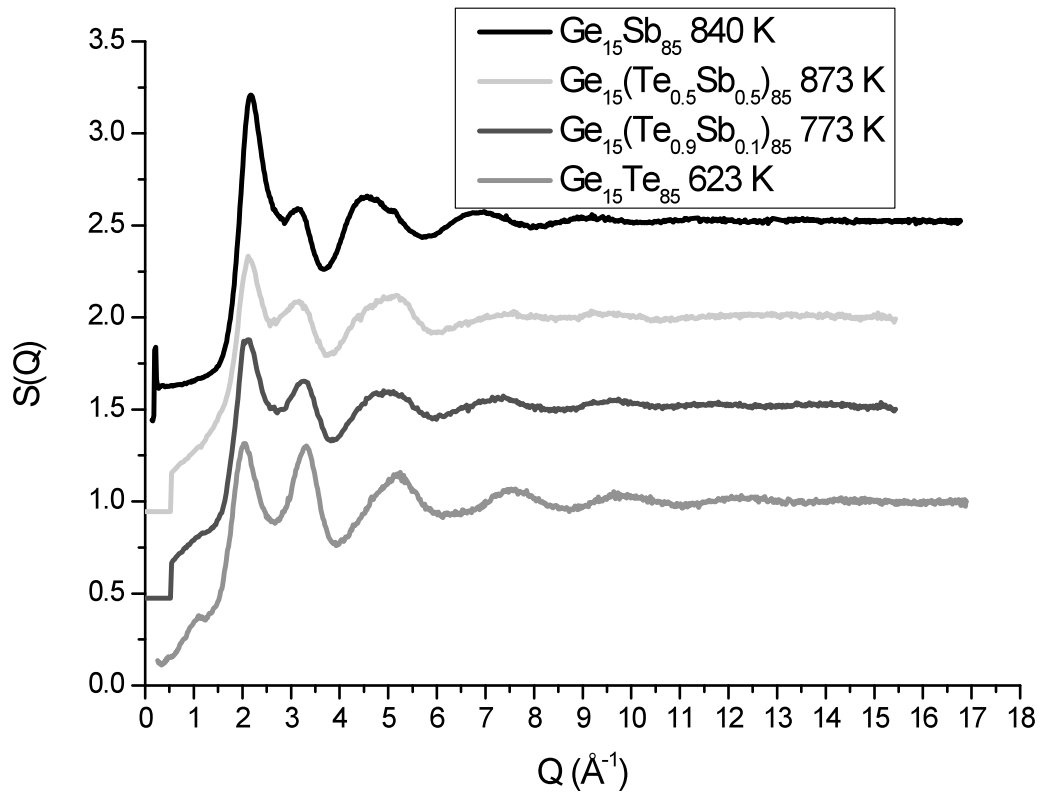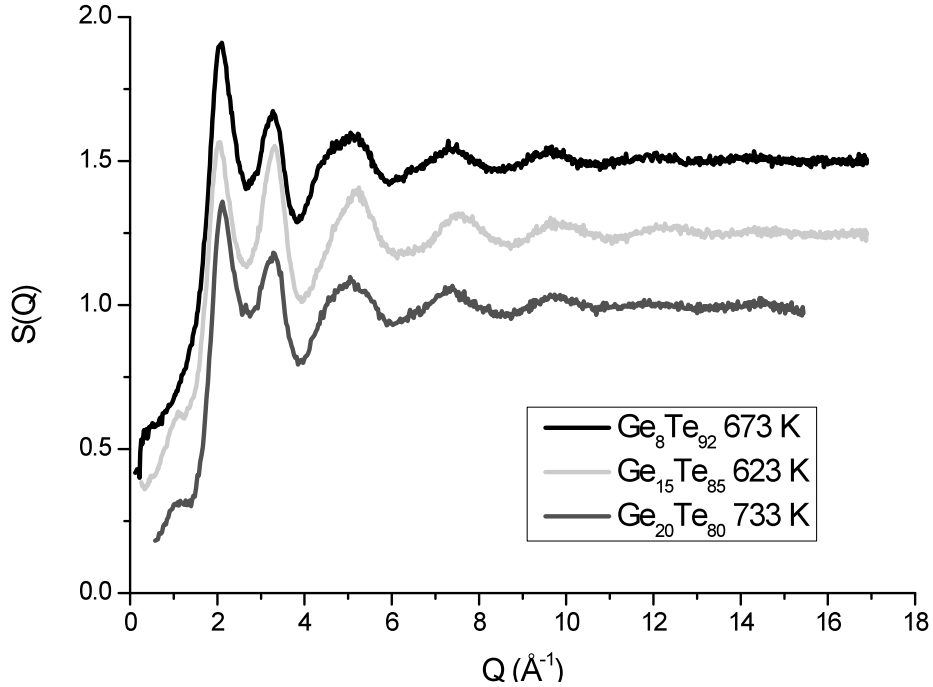**Figure 23: Structure factors S(Q) of Ge$_{15}$Te$_{85}$ at different temperatures (ref. 7)**

Figure 24: Structure factors S(Q) of different alloys at a temperatures above the liquidus. The first peak increases while the second peak decreases when the concentration of Sb increases.

In order to observe the impact of the variation of the concentrations of Ge and Te on the anomalies, $Ge_{15}Te_{85}$ can also be compared with $Ge_{20}Te_{80}$ and $GeTe_{12}$. Figure 25 shows the structure factors of those alloys just above their liquidus temperature.

Figure 25 : Structure factors of $Ge_{15}Te_{85}$, $Ge_{20}Te_{80}$ and Ge_8Te_{92}. When changing the concentration of Ge and Te in $Ge_{15}Te_{85}$, the second peak decreases.

First, it can be noticed on Figure 25 that a change in concentrations of Ge and Te, results in an increase of the melting temperature. It can be noticed that it has the same impact as adding Sb that is to say, the 'pre-peak' of $Ge_{15}Te_{85}$ seems to disappear and the two first peaks evolve.

5.2 The pair distribution functions

In order to calculate the pair distribution functions, the same cut-off function (equation (21)) was used for every studied sample and every temperature. The pair distribution functions of $Ge_{15}Te_{85}$, $Ge_{15}Sb_{85}$ and Ge_8Te_{92} were also calculated according to the structure factors obtained in previous studies, they are displayed in Appendix.
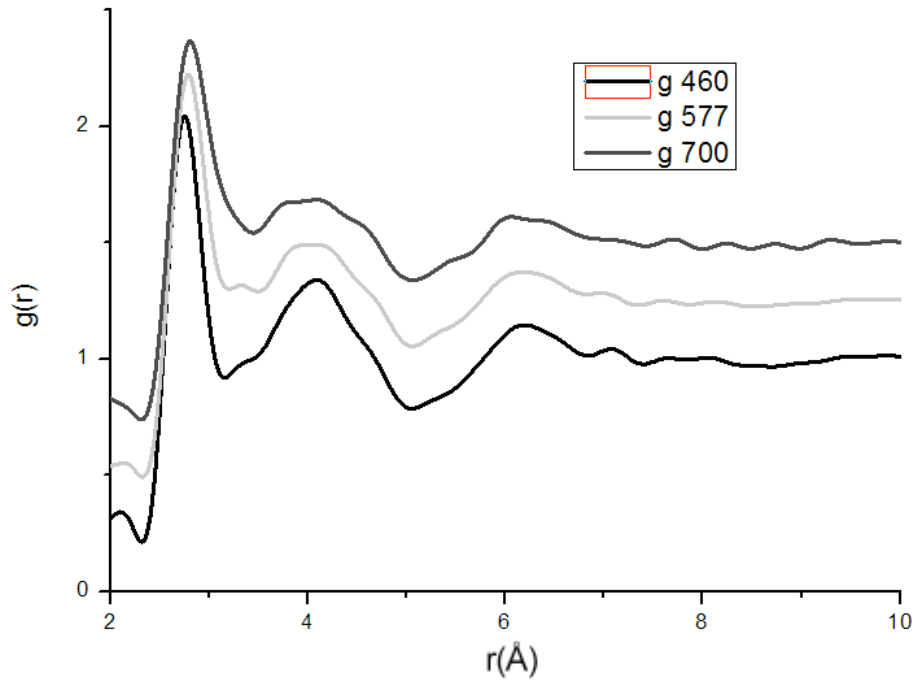
5.2.1 $Ge_{20}Te_{80}$

Figure 26 : Pair distribution function of Ge$_{20}$Te$_{80}$ at 3 temperatures T= 733 K, 850 K and 973 K

5.2.2 $Ge_{15}(Sb_{0.1}Te_{0.9})_{85}$

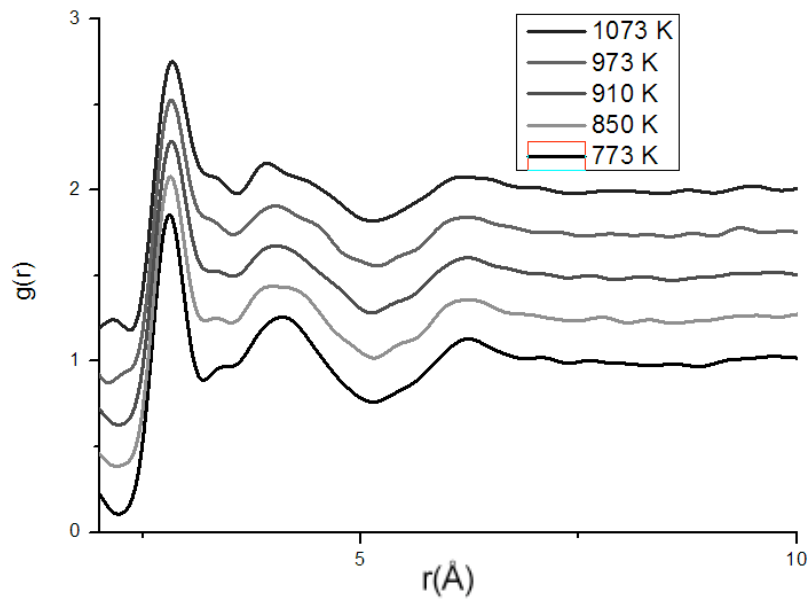**Figure 27 : Pair distribution function of Ge$_{15}$(Te$_{0.9}$Sb$_{0.1}$)$_{85}$ at 5 temperatures, T=773 K, 850 K, 910 K, 973 K ,1073 K**

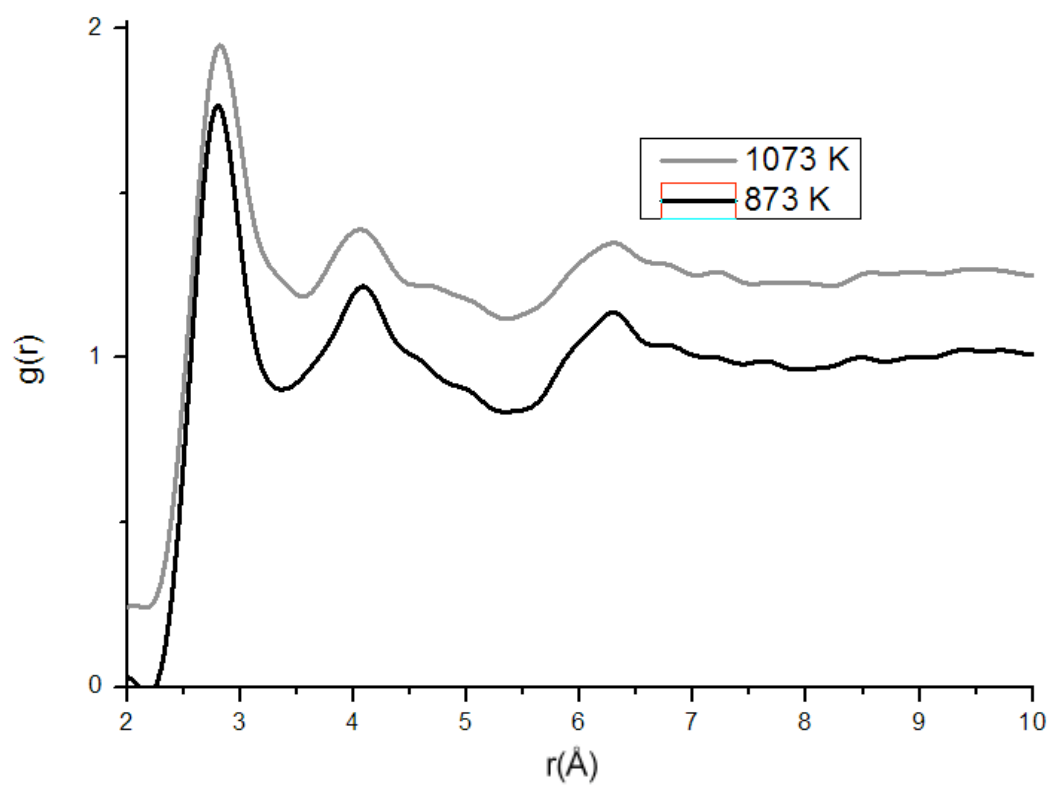### 5.2.3 $Ge_{15}(Sb_{0.5}Te_{0.5})_{85}$

Figure 28 : Pair distribution functions of Ge$_{15}$(Te$_{0.5}$Sb$_{0.5}$)$_{85}$ at 2 temperatures, T=873 K and 1073 K

5.3   Average Coordination Numbers

Average coordination numbers can be calculated by integrating the radial distribution function as described in 4.6.

The average coordination numbers for all studied sample as well as for $Ge_{15}Te_{85}$ and $Ge_{15}Sb_{85}$ are listed in the table below.

T(K)	$Ge_{15}Te_{85}$	T(K)	$Ge_{15}(Te_{0.9}Sb_{0.1})_{85}$	T(K)	$Ge_{15}(Te_{0.5}Sb_{0.5})_{85}$
623	2.1	773	2.48	873	2.74
643	2.13	850	2.57	1073	2.58
653	2.18	910	2.69		
685	2.25	973	2.66		
796	2.45	1073	2.64		

Table 1 : Average coordination numbers of $Ge_{15}Te_{85}$, $Ge_{15}(Te_{0.9}Sb_{0.1})_{85}$ and $Ge_{15}(Te_{0.5}Sb_{0.5})_{85}$ in their liquid state for the experimental temperatures

T(K)	$Ge_{15}Sb_{85}$	T(K)	$Ge_{20}Te_{80}$	T(K)	Ge_8Te_{92}
840	3.54	733	1.92	673	2.07
923	3.76	850	2.14	693	2.02
1023	3.4	973	2.43	723	2.13
				758	2.21
				813	2.13

Table 2 : Average coordination numbers of $Ge_{15}Sb_{85}$, $Ge_{20}Te_{80}$ and Ge_8Te_{92} in their liquid state for the experimental temperatures

The average coordination number increases when temperature increases as a result of the evolution of the distortion of the structure. It is also interesting to notice that the average coordination number has a tendency to increase when the concentration of Sb increases in $Ge_{15}Te_{85}$.

6   Discussion

For a polyatomic system, the total structure factor is a sum of the partial structure factors balanced with the scattering lengths and the atomic concentrations as defined in equation (9). There are as many partial factors as there are pair combinations between the atoms. In a binary system, such as $Ge_{15}Te_{85}$, there are 3 partial factors which are S_{GeGe}, S_{GeTe} and S_{TeTe}. In a ternary system, such as Ge-Te-Sb alloys, there are 6 partial factors. Then, the total structure factor gives global information about the system.

It can be noticed that the scattering lengths of Te and Sb have approximately the same value (Appendix 2). As a consequence, Ge-Sb-Te alloys can be approximately considered as a binary system composed of Ge atoms ($\bar{b} = 0.8185$) and of an average of Te and Sb atoms ($\bar{b} \approx 0.57$). As a consequence, when substituting Sb atoms to Te atoms, the scattering lengths distribution remains unchanged. As a result, an evolution of the total structure factors can only be explained by a change in the structure. As it was observed in the previous section, there is an evolution of the two first peaks of the structure factors as a function of temperature. In order to quantify this evolution, it was decided to study the ratio of the amplitudes of the two first peaks as a function of temperature for every composition. Those ratios are drawn on Figure 29.
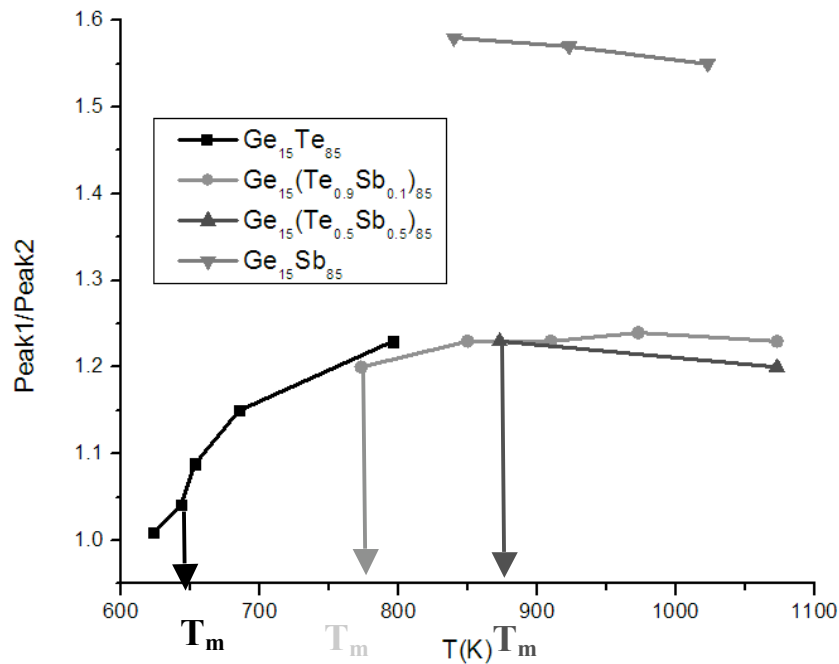

Figure 29 : Evolution of the ratio of the two first maxima of S(Q) as a function of temperature for $Ge_{15}Te_{85}$, $Ge_{15}(Te_{0.9}Sb_{0.1})_{85}$, $Ge_{15}(Te_{0.5}Sb_{0.5})_{85}$ and $Ge_{15}Sb_{85}$

Figure 29 clearly reveals a trend of the evolution of the two first maxima of S(Q) with temperature for the 3 first compositions. The assumption can be made that the alloys $Ge_{15}(Te_{1-x}Sb_x)_{85}$ with x<0.5 behave in the same way with temperature. As it was shown during simulations on $Ge_{15}Te_{85}$ (see Figure 4, ref. 6), this trend is representative of the evolution of the distorted octahedral structure with temperature.

It was thought at the beginning of the thesis that Sb was killing off the distortion (see 1.3). The anomaly of $Ge_{15}Te_{85}$ is situated under 760K (lowest point of the NTE on Figure 3). The melting point of $Ge_{15}(Te_{0.9}Sb_{0.1})_{85}$ (773 K) and $Ge_{15}(Te_{0.5}Sb_{0.5})_{85}$ (873 K) are both higher than

760 K. As a consequence, for those alloys, the anomaly would be located under their melting temperature and thus in the overcooled area. As a consequence, It seems that Sb would not kill off the distortion, as it was thought at the beginning of this thesis, but it would push back the anomaly into the overcooled area.

Although this curve seems to work universally for any composition between $Ge_{15}Te_{85}$ and $Ge_{15}(Te_{0.5}Sb_{0.5})_{85}$, $Ge_{15}Sb_{85}$ seems to behave in a completely different way.

The same kind of curve was obtained when comparing the ratio of the two first peaks of the structure factors of $Ge_{15}Te_{85}$, $Ge_{20}Te_{80}$ and $GeTe_{12}$ (Figure 30). The 3 curves seem to have the same shape but they are not stacked together due to the change in concentrations of Ge and Te which induces a change in the scattering lengths distribution. In fact, When changing the concentrations of both Ge and Te, the distribution in scattering length changes as b_{Ge} and b_{Te} are significantly different. The shape of each curve is the same as in Figure 29 and it reflects the evolution of the structure with temperature while the position of the curve is a result of the distribution in the scattering length. Nevertheless, the universally curve that resulted from Figure 29 seem to work. In this case as well, the melting points of $Ge_{20}Te_{80}$ and Ge_8Te_{92} are higher than $Ge_{15}Te_{85}$ and as a consequence the anomaly is, again, pushed back into the overcooled area for those alloys.

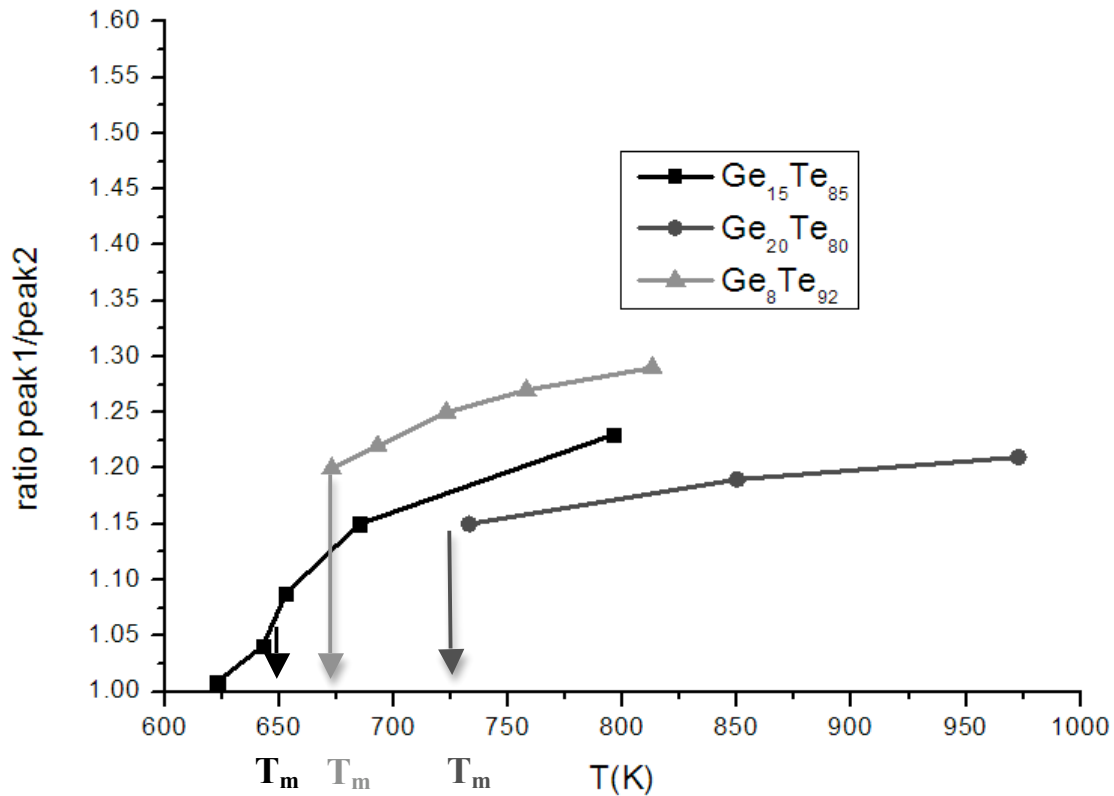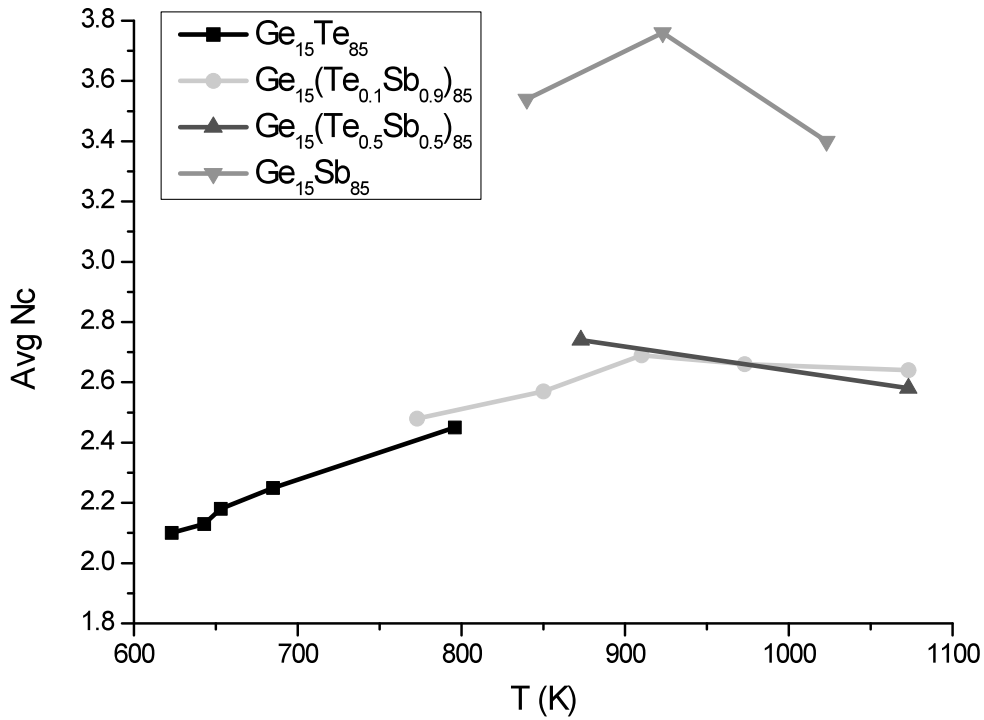**Figure 30: Evolution of the ratio of the two first maxima of S(Q) as a function of temperature for $Ge_{15}Te_{85}$, $Ge_{20}Te_{80}$ and $GeTe_{12}$**

The curves seem to tend towards a constant value, when the structure becomes more symmetric.

After these promising results, the evolution of the neighbouring atoms was studied with the average coordination numbers calculated in 5.3. Figure 31 shows the evolution in temperature of the coordination numbers for the different alloys.

Figure 31: Evolution of the average coordination number for different alloys as a function of temperature

The same kind of trend, as the one obtained before, can be noticed with the evolution of coordination numbers. Alloys from $Ge_{15}Te_{85}$ to $Ge_{15}(Te_{0.5}Sb_{0.5})_{85}$ seem to behave in the same way while $Ge_{15}Sb_{85}$ behaves differently.

The increase in the number of neighbouring atoms when temperature increases reveals the evolution of the distortion of the structure that becomes more symmetric when temperature increases

7   Development of experimental setup for the Inelastic X-ray measurements

The main work done on this experiment during the thesis was to develop a challenging sample containment. The container had to be thin enough so that the X-ray were not absorbed and thick enough to be able to introduce the sample in it. Of course, the sample should not leak and be sealed under vacuum. The results will not be shown in this report for this experiment, but all the work that was done behind the experiment will be described.

7.1   Purpose of the experiment

In addition to the thermodynamic anomalies, described in the introduction, $Ge_{15}Te_{85}$, also exhibits in the liquid state, above the melting point, an anomalous behaviour of the sound velocity in the liquid phase. Tsuchiya et al. have measured this anomalous propagation in Te rich Ge-Te alloys (see Figure 32) (ref. 5).
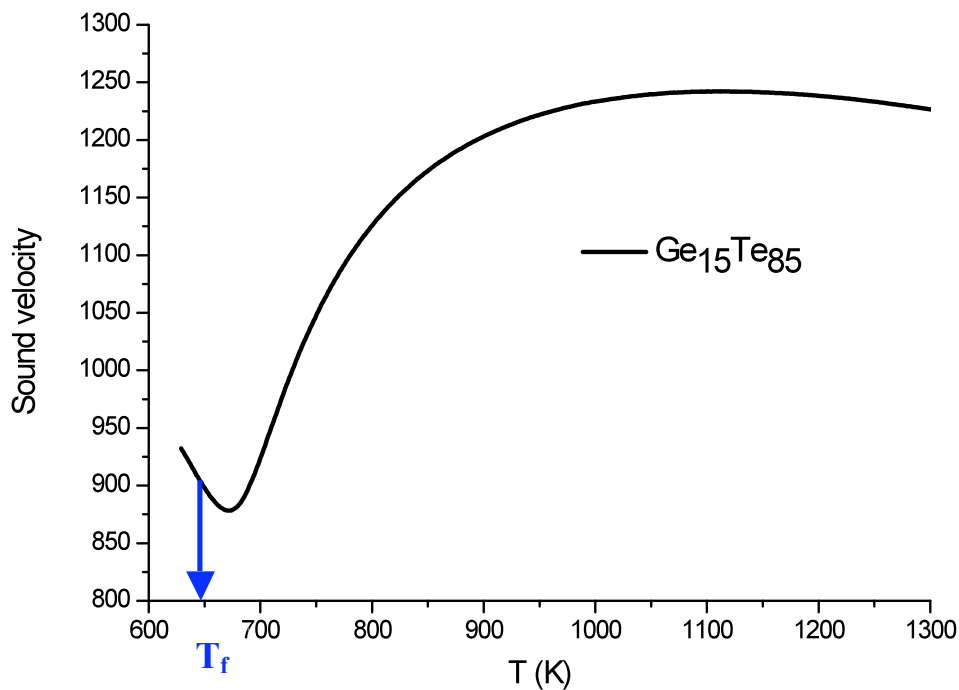

Figure 32 : Anomalous behaviour of the sound velocity in liquid $Ge_{15}Te_{85}$
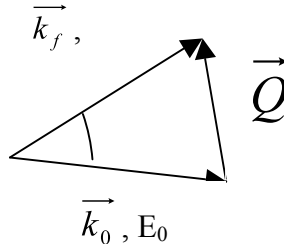
The goal of the experiment was to measure the inelastic energy transfer in a sample of $Ge_{15}Te_{85}$ in the liquid state.

7.2   Technique principle

IXS permits the study of atom dynamics in condensed matter through the measurement of the energy and wave vector of excitations. It is especially useful to study disordered materials since it gives access to small wave vectors.
Various properties of a material are accessible by IXS such as sound velocities.

As in section 2.1.1., for neutron scattering, the scattering triangle is defined, but now one considers the energy of the scattered beam.

The energy transfer is defined as $\Delta E = E_f - E_0$ with E_f the energy of the scattered beam and E_0 the energy of the incident beam. For X-Rays, the incident energy is given by: $E_0 = h\nu = \dfrac{hc}{\lambda}$. For the experiment the wavelength was $\lambda = 0.5226\,\text{Å}$, then

$E_0 = \dfrac{12.398}{0.5226} = 23.724\,\text{keV}$.

The energy transfer is typically equal to a few meV. As a consequence, $\Delta E << E_0$. Using X-rays to measure energy transfer requires the use of an incident beam with an extremely well defined energy.

7.3   Beamline layout

The experiments were performed at the European Synchrotron Radiation Facility (ESRF) situated in Grenoble (France) on beamline ID28. The general optical layout of the spectrometer and the distances involved are given on Figure 33.
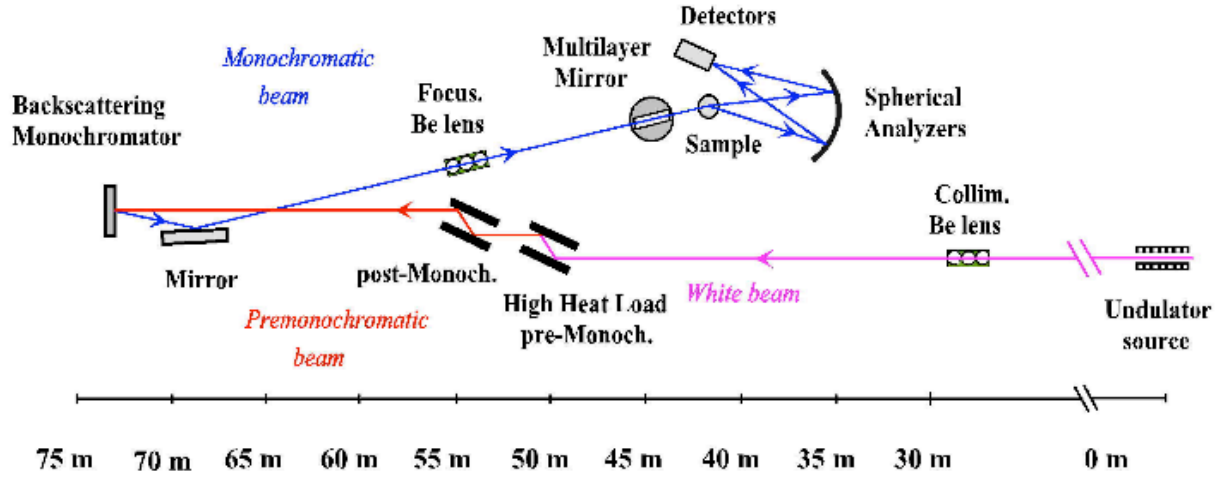

Figure 33 : Optical layout of the beamline ID28 at ESRF, Grenoble (FRANCE) (http://www.esrf.eu/)

The most important particularity of this experimental setup is the succession of monochromators which is necessary in order to reach the required high energy resolution. The pre-monochromator is a crystal of Si (1, 1, 1) which gives a energy resolution of $\frac{\delta E}{E} = 2.10^{-4}$. A Si (3 3 1) is used for the post-monochromator, which provides an intrinsic energy resolution of $\frac{\delta E}{E} = 1.44.10^{-5}$. The main monochromator uses a close-to-exact-backscattering configuration (89.98°); it consists of a flat perfect single crystal of Si (12, 12, 12). This results in a high energy resolution of $\frac{\delta E}{E} = 4.7.10^{-8}$. There are 8 analysers positioned at different angles, as a consequence each of them corresponds to a given value of Q. Then, in each experiment, the signals for 8 values of Q are measured simultaneously. The analysers cannot be moved independently. During the experiment, the measurements were performed at two different Qsets for angles going from 1° to 7°. The X-Ray beam, used during the experiment, was 50µm high and 200µm wide.

7.4   Containment of the sample

The initial $Ge_{15}Te_{85}$ ingot was crushed into small grains. A challenging sample design had to be imagined for this experiment. Indeed, due to the high absorption of X-rays, the sample thickness could not exceed 300µm. Besides it had to be contained in the thinnest possible container and be sealed under vacuum to protect from oxidation. Of course the liquid must not leak. A first attempt was made with a design consisting of slices of sapphire and silica sealed with glue. This first design was thin enough to be used in IXS but it failed to contain the material when melted. A second attempt was to adapt the design (see section 2.2.3.) of the container used for neutron scattering experiments at a much reduced scale. In order to do so, capillaries made of amorphous SiO_2 were used (inner diameter 300 µm, outer diameter 320 µm). After breaking the initial material into small grains, the capillary was filled up and finally it was sealed, under vacuum, with a blowtorch. The challenge was to fill enough powder into the capillary so that when melted enough liquid is in the X-Ray beam. This final design succeeded to contain the sample when melted and no leakage was recorded during the experiment (total time 5 days). Figure 34 depicts the setup used.
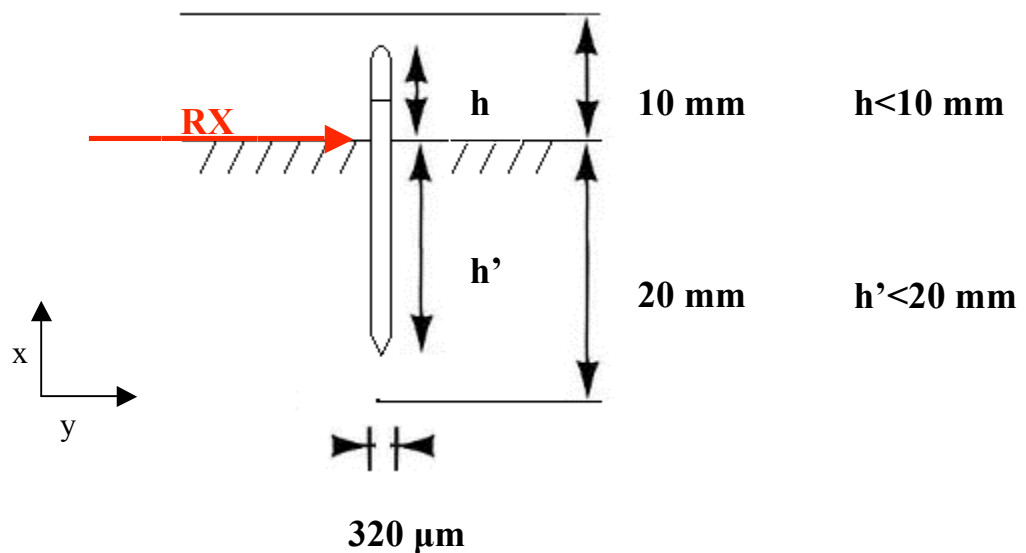

Figure 34: Final sample design for IXS experiment

The sample was studied, in the liquid state, at 3 different temperatures, T=800 K, 620 K and 700 K. The temperatures were chosen from Figure 3 in order to be in the area of the NTE.
A thermocouple, placed close to the mounting of the sample, was used to measure the temperature in the furnace. The thermocouple was not place close to the sample, in order not to be in the way of the X-Ray beam. Then, the furnace was calibrated after the experiment (Appendix 5).

7.5   Evaluation of the size of the droplet

As the container of the sample was rather small, the sample could not flow properly, then the measured sample was in reality a droplet that does not occupy the whole width of the container.

The transmission coefficient was measured with a beam size of 50 μm which is smaller than the one used during the experiment, to ensure that the beam contained the whole droplet. A scanning of the sample is done on the y-direction as described on Figure 35. The result of the scan is shown on Figure 36.
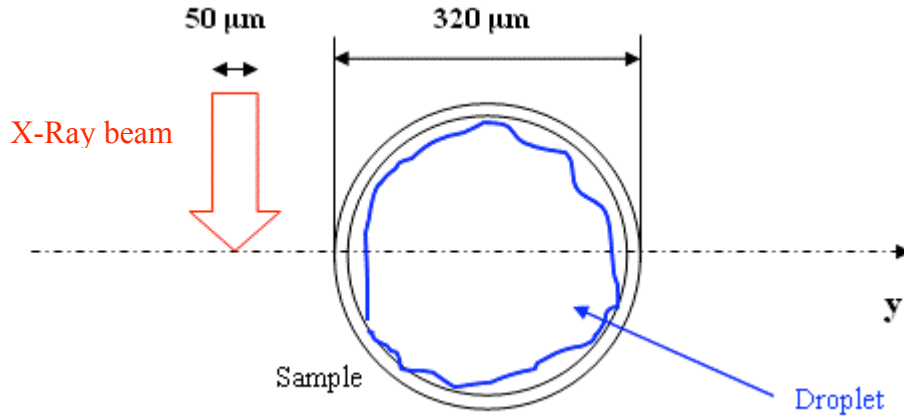

Figure 35: Scan in the y direction of the droplet under a 50 μm X-Ray beam

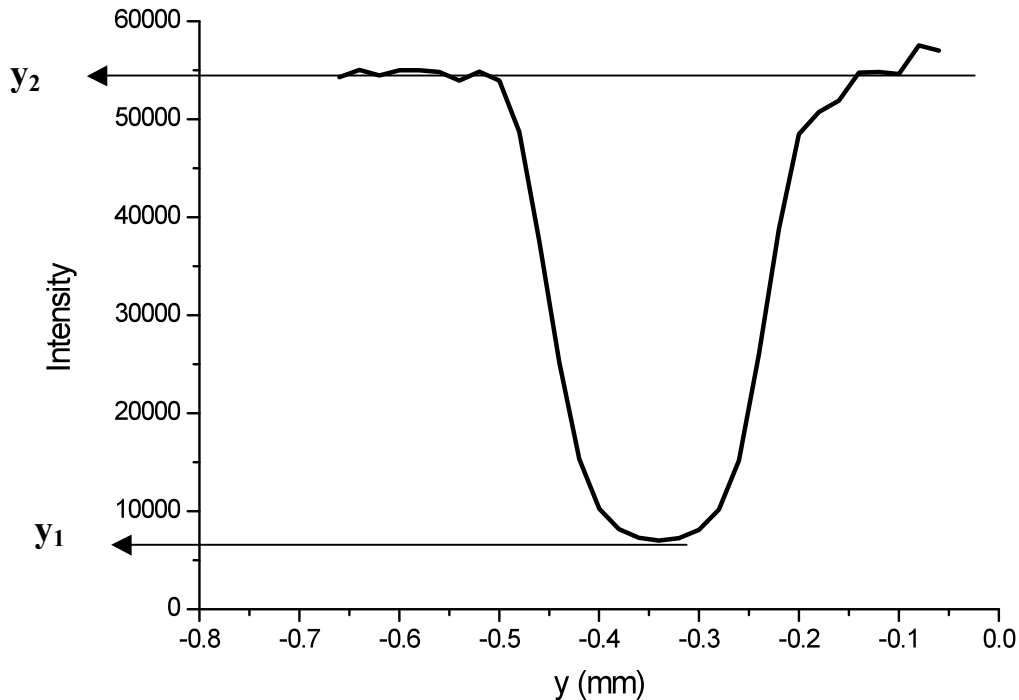**Figure 36: Transmission of the droplet under a 50 μm X-Ray beam**

The transmission at the centre of the droplet is $T = \dfrac{y_1}{y_2} = 0{,}13$.

If it is considered that the transmission follows the rule

$$T = \exp(-\mu_{Ge15Te85}x) \qquad (23)$$

where $\mu_{Ge15Te85}$=92.9 cm^{-1} is the absorption coefficient of Ge$_{15}$Te$_{85}$ calculated in Appendix 3. x is the size of the sample.

Then, $x = -\dfrac{\ln(0.13)}{92.9} = 0.022$ cm=220 μm

If one considers the droplet as spherical, which is likely due to the symmetric shape of the transmission curve, its diameter is 220 μm.

8   Conclusion

The work done and the experiments performed during this thesis lead to promising results. The work was divided in two parts, a new design to perform inelastic experiment was invented to study Ge-Sb-Te liquids and neutron scattering experiments were performed in order to study the structure of those same liquids.

First, a design had to be made in order to study the dynamics of liquids by Inelastic X-Ray scattering. This design was challenging for many reason. Indeed, this experiment is a first of a kind, so a new sample containment had to be designed following strict requirements with dimensions constraints for the containing cell. This design was a success because some results were obtained, even if those results are not exploitable or publishable it is promising for future experiments of this kind. The final design of the container was a capillary made of amorphous SiO_2 (inner diameter 300 µm, outer diameter 320 µm) sealed under vacuum.

Second, neutron scattering experiments were performed in order to study the structure of some Ge-Sb-Te alloys in their liquid state. Those experiments were success but they lead, somehow, to unexpected conclusions. In fact, the purpose of these experiments was, at the beginning, to study how Sb was killing off the anomaly that was found in the structure of $Ge_{15}Te_{85}$ during previous studies. In order to study this, three different compositions were studied, $Ge_{15}(Te_{0.9}Sb_{0.1})_{85}$, $Ge_{15}(Te_{0.5}Sb_{0.5})_{85}$ and $Ge_{20}Te_{80}$. At the end, it was found that Sb does not kill off the anomaly but that it pushes it back into the overcooled area. In fact, the melting point is increased when Sb is added into the structure. As a consequence, the anomaly can only be seen in the liquid state of $Ge_{15}Te_{85}$ which has the lowest melting point. It was revealed that the structure of the alloys going from $Ge_{15}Te_{85}$ to $Ge_{15}(Sb_{0.5}Te_{0.5})_{85}$, in the liquid state, behave in the same way with temperature but $Ge_{15}Sb_{85}$ seemed to behave differently. As a consequence, a 'universal behaviour' seems to work for $Ge_{15}(Sb_xTe_{1-x})_{85}$ alloys with $0<x<0.5$, while what happens for alloys with $x>0.5$ remains uncertain.
This behaviour is characteristic of the evolution of the distortion when temperature increases.

As a result, $Ge_{15}Te_{85}$ and $Ge_{15}Sb_{85}$ behave in totally different ways. But, it is interesting to notice that in the past, both $Ge_{15}Te_{85}$ and $Ge_{15}Sb_{85}$ have been suggested as potential PCM due to their rapid phase transition between the amorphous and the crystal phases and their good cyclability. So how can these two alloys, which seem to have completely different behaviours in temperatures, be potential phase change materials?

In order to totally understand the structural changes happening in those alloys, ab initio simulations are necessary. Simulations have already been performed on $Ge_{15}Te_{85}$ and $Ge_{15}Sb_{85}$ during previous studies. A distortion of the octahedral structure was revealed around Ge atoms in $Ge_{15}Te_{85}$ (see Figure 3). It appears that Ge has three short and three long bonds that become symmetric when temperature increases. Conversely, this distortion disappears in $Ge_{15}Sb_{85}$. To go beyond and to have a better understanding of the effect of substituting Sb to Te atoms in $Ge_{15}Te_{85}$, simulations are in progress on the alloy $Ge_{15}(Te_{0.5}Sb_{0.5})_{85}$. Further experiments performed on other alloys on the line between $Ge_{15}Te_{85}$ and $Ge_{15}Sb_{85}$ (Figure 1) would also help to understand the structural changes.

9   Acknowledgements

10   References

1 Wuttig, M. and Yamada, N. 2007, 'Phase-change materials for rewriteable data storage', *Nature Materials*, 6, 824-832.

2 Wuttig, M. and Steimer, C. 2007, 'Phase-change materials: From materials science to novel storage devices', *Applied Physics A: Materials Science & Processing*, 87 (3), 411-417.

3 Bletskan, D. I. 2005, 'PHASE EQUILIBRIUM IN THE SYSTEMS AIV – BVI', *Journal of Ovonic Research*, 1 (5), 53 – 60

4 Bergman, C. et al. 2003, 'Experimental investigation of the waterlike density anomaly in the liquid $Ge_{15}Te_{85}$ eutectic alloy', *Physical Review B*, 67 (10), 104202.1-104202.5

5 Tsuchiya, Y. 1991, 'the anomalous negative thermal expansion and the compressibility maximum of molten Ge-Te alloys', *Journal of the physical society of Japan*, 60 (1), 227-234

6 Raty, J.-Y. et al. 2003, 'Properties of molten Ge chalcogenides: an ab initio molecular dynamics', *Journal of Physics Condensed Matter*, 15, 167-173

7 Otjacques, C. 2010, PHD thesis, Université de Liège, unpublished

8 Fisher, H. E. et al. 2006, 'Neutron and x-ray diffraction studies of liquids and glasses', *Reports on Progress in Physics*, 69, 233-299

9 Varley F. Sears 1992 Neutron News 3, 26, the same information is available at http://www.ncnr.nist.gov/ressources/n-lengths.

10 Paalman, H.H. et Pings C.J. 1962, 'Numerical evluation of X-ray absorption factors for cylindrical samples and an- nular sample cells', *Journal of Applied Physics*, 33(8), 2635-2639

11 Blech I.A. et Averbach B.L. 1965, 'Multiple scattering of Neutrons in Vanadium and Copper', *Physic Review*, 137, pp. 1113-1116

12 Placzeck, G. 1952, *Physic Review,* 86 (3), 377

Appendix 1: Densities

In order to measure the Fourier Transform of the structure factors it is necessary to know the density of the alloys which were studied. Since no measures are available, the densities of the alloys Ge-Sb-Te have been calculated from the molar volume measurements of Tsushiya Y. (ref. 5) and from the density expressions of pure elements Ge, Sb and Te found in literature. Tsushiya Y. measured the density of the pure element Te as a function of temperature (Figure 37).

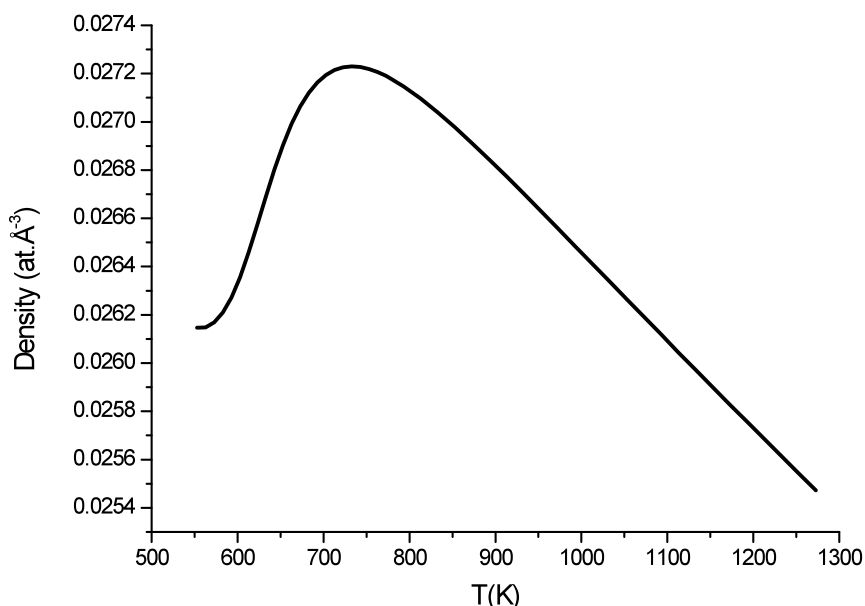**Figure 37: density of Te measured by Tsuchiya Y.**

An average of the expressions found in the handbook for the densities of pure elements Ge and Sb is represented on Figure 38. Those representations are representative just above the melting points of Ge and Sb.
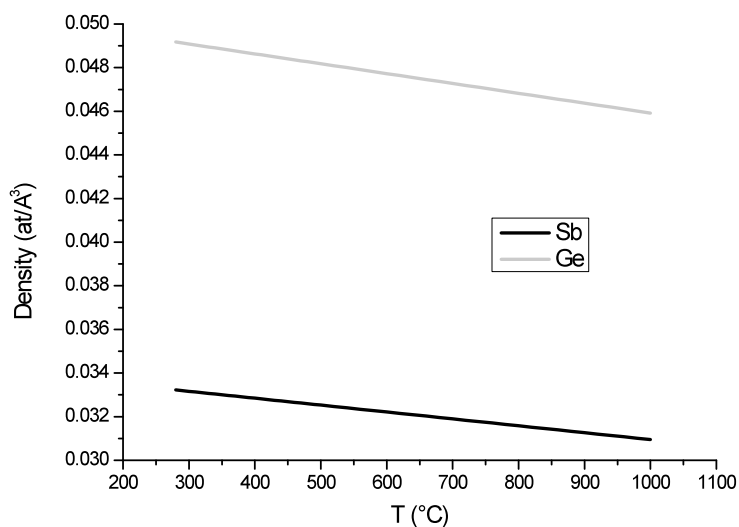

Figure 38: Densities of pure elements Ge and Sb

The densities of the studied alloys can be approximated from these data.

43

The densities in at/Å^3 used for the neutron scattering corrections are indicated in the table bellow.

Ge$_{15}$(Te$_{0,9}$Sb$_{0,1}$)$_{85}$		Ge$_{15}$(Te$_{0,5}$Sb$_{0,5}$)$_{85}$		Ge$_{20}$Te$_{80}$	
T (K)	ρ (at/Å^3)	T (K)	ρ (at/Å^3)	T (K)	ρ (at/Å^3)
773	0,0314	873	0,0310	733	0,0298
850	0,0312	1073	0,0303	850	0,02955
910	0,0310			973	0,0291
973	0,0308				
1073	0,0304				

Table 3: Densities for the studied alloys at the temperatures of the neutron scattering experiment

The variation of the density with temperature is rather small (of the order of magnitude of 1%).

The density of the amorphous SiO$_2$ container that was taken for the corrections is $\rho = 0.0662 \text{ at/Å}^3$.

Tsuchya Y. also measured the density of Ge$_{15}$Te$_{85}$ as a function of temperature. The densities in g/cm^3 at the temperatures of the IXS experiment are given in the table below.

Ge$_{15}$Te$_{85}$	
T (K)	ρ (g/cm^3)
680	5.62
760	5.73
860	5.69

Table 4: Densities of Ge$_{15}$Te$_{85}$ at the temperatures of the IXS experiment

Appendix 2: Cross sections and neutron scattering lengths

The neutron scattering lengths and cross sections for the different elements can be found on the website http://www.ncnr.nist.gov/.

	σ_{scatt}	σ_{coh}	σ_{incoh}	σ_{abs}	σ_{abs}	σ_{tot}	b_{coh}
Ge	8.60	8.42	0.18	2.20	0.885	9.485	0.8185
Te	4.32	4.23	0.09	4.70	1.89	6.21	0.580
Sb	3.9	3.9	0.007	4.91	1.975	5.875	0.557
Si	2.167	2.163	0.004	0.171	0.6878	2.236	4.149
O	4.232	4.232	0.0008	0.00019	0.000076	4.232	5.803

Table 5: Cross sections and scattering lengths for the three elements Ge, Sb, Te

The cross sections are expressed in barns (1barn=10^{-24}cm^2).

σ_{coh} and σ_{incoh} are the coherent and incoherent cross sections resulting from coherent and incoherent scattering.

σ_{scatt} is the scattering cross section, $\sigma_{scatt} = \sigma_{coh} + \sigma_{incoh}$.

σ_{abs} is the absorption cross section. σ_{abs} is known for a wavelength of 1.8 Å. It is necessary to calculate it for the wavelength of the experiment which was 0.724 Å. Then:

$$\sigma_{abs}(0.724 A) = \frac{\sigma_{abs}(1.8 A) * 0.724}{1.8}$$

σ_{tot} is the total cross section, $\sigma_{tot} = \sigma_{scatt} + \sigma_{abs}$.

The scattering lengths are expressed in femtometer (1fm=10^{-15}m).
bcoh is the coherent scattering length.

From those data, it is possible to calculate the same parameters for every Ge/Sb/Te alloys.

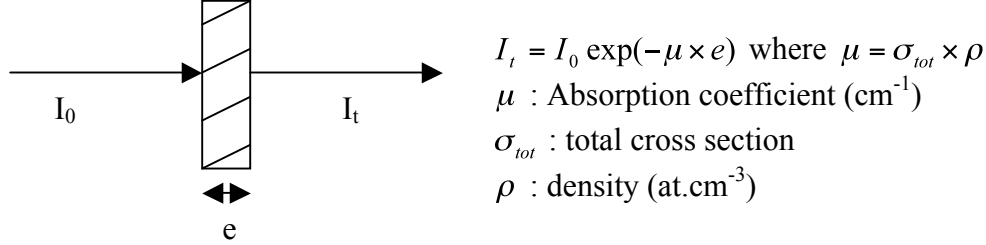|	σ_{scatt}	σ_{abs}	σ_{tot}	$b_{coh} = \bar{b}$	$\bar{b}^2$	$\overline{b^2}$
Ge$_{15}$(Te$_{0,9}$Sb$_{0,1}$)$_{85}$	4.926	1.741	6.667	0.614	0.377	0.392
Ge$_{15}$(Te$_{0,5}$Sb$_{0,5}$)$_{85}$	4.784	1.770	6.554	0.606	0.367	0.381
Ge$_{20}$Te$_{80}$	5.176	1.689	6.865	0.628	0.394	0.412
SiO$_2$	3.543	0.229	3.772	5.252	27.58	0.282

Table 6: Cross sections and scattering lengths for the studied alloys

In order to calculate $\overline{b^2}$, the following equation is used: $\sigma_{scatt} = 4\pi \overline{b^2}$.

Appendix 3: Absorption coefficients

a.   Neutron absorption coefficients

In a simple case of a rectangular sample, the absorption can be defined as following:

$I_t = I_0 \exp(-\mu \times e)$ where $\mu = \sigma_{tot} \times \rho$

μ : Absorption coefficient (cm^{-1})

σ_{tot} : total cross section

ρ : density (at.cm^{-3})

The absorption coefficients of the studied alloys, for the neutrons can be calculated from the density values calculated in Appendix 1 and the total cross section values calculated in Appendix 2.

Ge$_{15}$(Te$_{0,9}$Sb$_{0,1}$)$_{85}$		Ge$_{15}$(Te$_{0,5}$Sb$_{0,5}$)$_{85}$		Ge$_{20}$Te$_{80}$	
T (K)	μ (cm^{-1})	T (K)	μ (cm^{-1})	T (K)	μ (cm^{-1})
773	0.209	873	0.203	733	0.205
850	0.208	1073	0.199	850	0.203
910	0.207			973	0.200
973	0.205				

Table 7: Absorption coefficients

The variation of the absorption coefficients with temperature is small (of the order of magnitude of 1%).

b.   X-Ray absorption coefficients

The values of $\dfrac{\mu}{\rho}$ for each element can be found on the website http://csrri.iit.edu/mucal.html.

For Ge and Te, it gives $\left(\dfrac{\mu}{\rho}\right)_{Ge} = 26.28\,\text{cm}^2/\text{g}$ and $\left(\dfrac{\mu}{\rho}\right)_{Te} = 14.57\ \text{cm}^2/\text{g}$.

Considering that $\dfrac{\mu}{\rho} = \sum_i w_i \left(\dfrac{\mu}{\rho}\right)_i$, one can calculate:

$$\left(\dfrac{\mu}{\rho}\right)_{Ge15Te85} = \dfrac{15}{100}\left(\dfrac{\mu}{\rho}\right)_{Ge} + \dfrac{85}{100}\left(\dfrac{\mu}{\rho}\right)_{Te} = 16.33\ \text{cm}^2/\text{g}$$

The absorption coefficients were calculated with the densities from Appendix 1.

Ge$_{15}$Te$_{85}$	
T (K)	μ (cm^{-1})
680	91.77
760	93.57
860	92.92

Table 8: Absorption coefficients at the temperatures of the IXS experiment

Appendix 4: Structure factors of Ge$_{15}$Sb$_{85}$ et GeTe$_{12}$

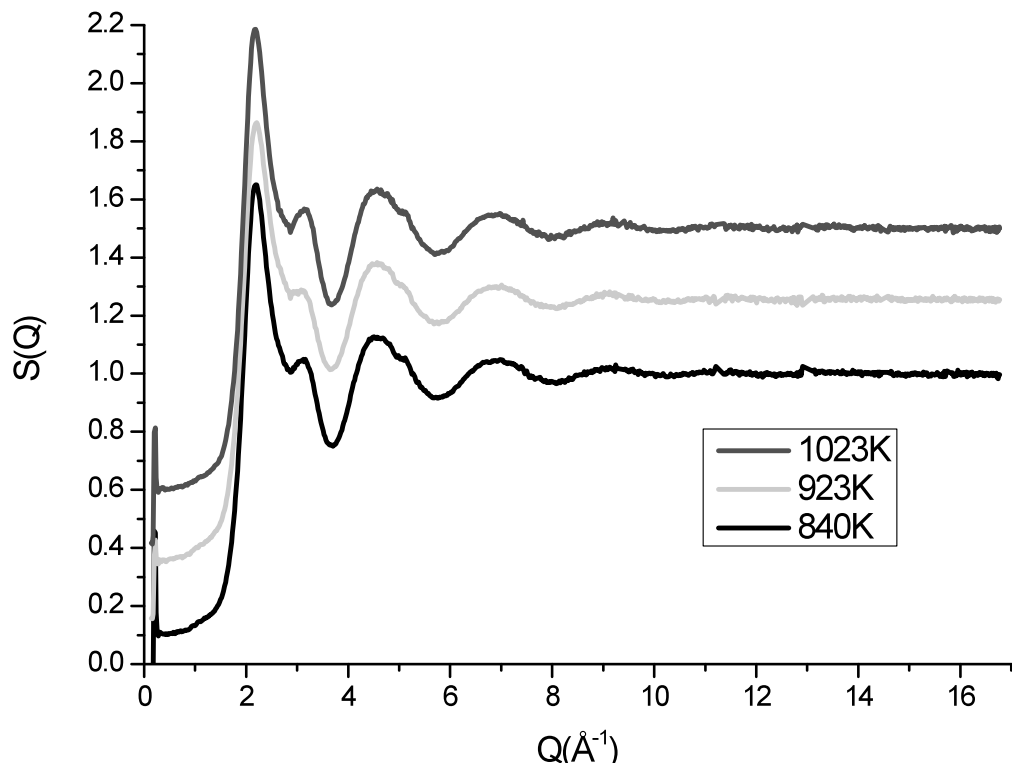**Figure 39: S(Q) of Ge$_{15}$Sb$_{85}$**

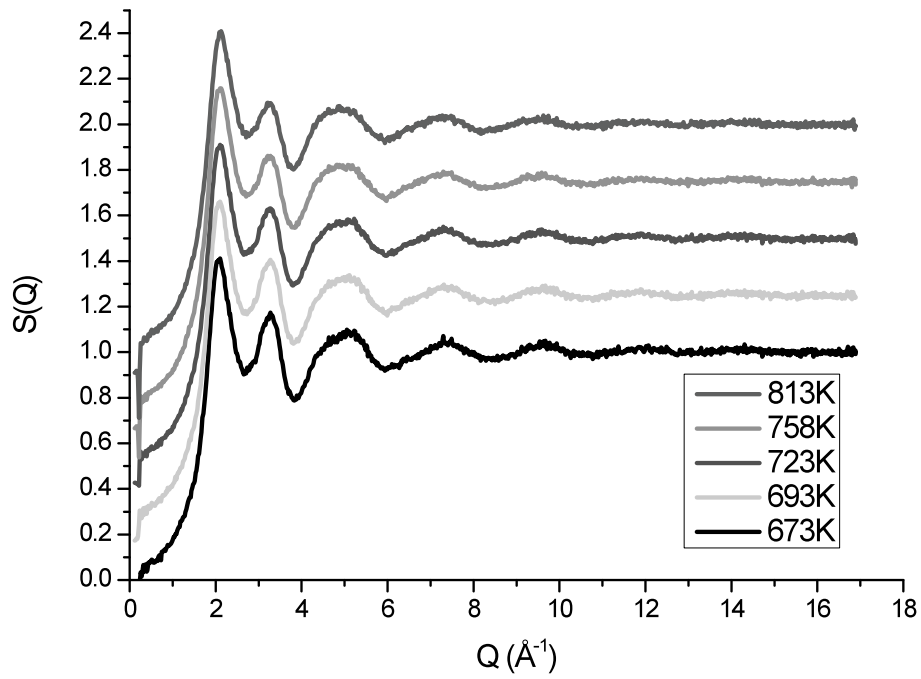**Figure 40: S(Q) of Ge$_8$Te$_{92}$**

Appendix 5: Furnace calibration

Once the sample was liquid, the temperature was decreased slowly in order to see whether the sample could be overcooled. According to the thermocouple used for the experiment, the sample crystallised at a temperature of $T_{m\ exp}$=590 K. Nevertheless, the well-known melting temperature of $Ge_{15}Te_{85}$ is $T_{m\ lit}$=650 K.

The thermocouple was not in contact with the sample during the experiment then, it could result in a misinterpreted temperature. The voltage and intensity values corresponding to some temperatures were noted during the experiment. A calibration of the furnace at the same power was then done after the experiment, in the same conditions to those of the experiment but this time the thermocouple was glued in contact with the sample.

T_{exp} (K)	U (V)	I (A)	T_{calib} (K)
590	2.66	14	693
620	2.82	15	726
700	3.25	18	800
800	3.85	21	840

Table 9: Experimental temperatures and calibration temperatures

Where T_{exp} is the experimental temperature, T_{calib} is the calibration temperature, U and I the voltage and the intensity of the power-regulated furnace.

During the calibration, for the same power of the furnace, higher temperatures were measured and it was noticed that there was a constant difference of ~100 K (T_{exp}-T_{calib}).

If the calibration temperatures are considered as the real temperatures, it would mean that the melting temperature was measured at 690 K ($T_{m\ exp}$+100K).

This would be again contradictory with $T_{m\ lit}$.

Then, it was considered that the real melting temperature was 650 K (as known from literature) instead of the measured 590 K. It was shown during the calibration that the difference between the experimental temperatures T_{exp} and the calibration temperatures T_{calib} was a constant. It was decided that this constant was equal to 60 K in reality (650-590). Then, T_{real}=T_{exp}+60.

As a consequence, the measurement temperatures would be T_{real}=860 K, 680 K and 760 K.